FP7-600716

Whole-Body Compliant Dynamical Contacts in Cognitive Humanoids

D4.3
Learning of the prioritization policies.

Editor(s)	Jan Peters[1,2] and Elmar Rueckert[1]
Responsible Partner	TUDA
Affiliations	[1] Intelligent Autonomous Systems Lab, Technische Universität Darmstadt, 64289 Darmstadt, Germany. [2] Robot Learning Group, Max-Planck Institute for Intelligent Systems, Tuebingen, Germany.
Status-Version:	Draft-1.0
Date:	Feb. 28, 2017
EC Distribution:	Consortium
Project Number:	600716
Project Title:	Whole-Body Compliant Dynamical Contacts in Cognitive Humanoids

Title of Deliverable:	Learning of the prioritization policies.
Date of delivery to the EC:	28/2/2017

Workpackage responsible for the Deliverable	WP4
Editor(s):	Jan Peters and Elmar Rueckert
Contributor(s):	Ryan Lober, Vincent Padois, Olivier Sigaud, Valerio Modugno, Gerhard Neumann, Elmar Rueckert, Giuseppe Oriolo, Jan Peters, Serena Ivaldi, Alex Paraschos, Ugo Chervet
Reviewer(s):	
Approved by:	All Partners

Abstract	The scope of the current deliverable is to present the results on the learning of the task prioritization policies.
Keyword List:	contacts, inverse dynamics model learning, probabilistic movement representations, reinforcement learning

Document Revision History

Version	Date	Description	Author
v. 0.1	Feb. 07	Initial Draft	Elmar Rueckert
v. 0.2	Feb. 20	Draft	Elmar Rueckert
v. 1.0	Feb. 21	Final	Elmar Rueckert

Table of Contents

Chapter 1

Introduction

This deliverable presents results of task T4.4. In total four articles were presented at international robotics conferences (HUMANOIDS, ICRA and IROS) and two articles are currently under review. Below, we discuss the achievements with respect to the task description from the Technical Annex.

1.1 Task description from the Technical Annex.

The core element of WP3 is the intelligent combination of prioritized tasks, which allows covering a large variety of possible scenarios while only requiring a small number of elements. Nevertheless, WP3s architecture requires a meaningful prioritization scheme that tells the systems which tasks to activate and how certain tasks can overrule each other. While it is possible to devise such prioritizations for complex tasks manually (see, e.g., Sentis et al., 2008), the automatic generation from data is much more desirable. Hence, in this task, we will investigate how a prioritization can be obtained from observing tasks, similar as in imitation learning, and how it can be self-improved. The relative importance of the tasks imposed by the prioritization can be changed during execution by the learned prioritization based on the current context. First, T4.4 will only help reproduce behavior from WP2 on the iCub but subsequently, it will allow for generalization to novel situations. Expected task outcomes are the following:

- Objective 1: A learned importance weighting for elementary tasks; weighting will allows appropriate combinations to generate solutions for new, more complex scenarios.
- Objective 2: A learned prioritization policy using both imitation and reinforcement learning (see tasks from WP2); demonstration and generalization to novel situations.

1.2 Contributions within the CoDyCo consortium.

We developed learning approaches that avoid task interferences prior to the task execution, that can be trained through reinforcement learning from a general task objective and from imitation learning in a probabilistic model.

- To objective 1: At UPMC, efficient whole-body control strategies have been developed that avoid interferences of multiple task objectives prior to a task execution. Two articles were published at international conferences and are summarized in Chapter 2. A detailed description can be found in *Deliverable D3.3*.
- To objective 2: In a collaboration, INRIA and TUDA studied the learning of task priority profiles for whole-body control. We optimized the parameters of priority profiles with respect to a general task objective through reinforcement learning [4]. This work is presented in Chapter 3.
  In a followup study, INRIA investigated different stochastic search implementations for reinforcement learning [5]. An article on the approach is listed in Chapter 4.
  In another study, TUDA investigated how task such priority profiles can be obtained from imitation learning. A research article of this study is currently under review [6]. In Chapter 5, we present a draft of this contribution.

Chapter 2

Multiple Task Learning for Whole-Body Reactive Control (UPMC)

In the following three paragraphs, we summarize the work of Ryan Lober, Vincent Padois and Olivier Sigaud on learning the task prioritization of multiple tasks. For a detailed report on these two articles we refer to *Deliverable D3.3*.

Multiple Task Optimization using Dynamical Movement Primitives for Whole-Body Reactive Control. Whole-body controllers provide the tools to execute multiple simultaneous tasks on humanoid robots, but given the robots internal and external constraints, interferences are often generated which impede task completion. Priorities can be assigned to each task to manage these interferences, unfortunately, this is often done at the detriment of one or more tasks. In this paper we present a novel framework for defining and optimizing multiple tasks in order to resolve potential interferences prior to task execution and remove the need for prioritization. Our framework parameterizes tasks with Dynamical Movement Primitives, simulates and evaluates their execution, and optimizes their parameters based on a general compatibility principle, which is independent of the robots topology, tasks or environment. Two test cases on a simulation of a humanoid robot are used to demonstrate the successful optimization of initially interfering tasks using this framework.

This work was presented at the international conference on humanoid robots [1].

Variance Modulated Task Prioritization in Whole-Body Control. Whole-Body Control methods offer the potential to execute several tasks on highly redundant robots, such as humanoids. Unfortunately, task combinations often result in incompatibilities which generate undesirable behaviors. Prioritization techniques can prevent tasks from perturbing one another but often to the detriment of the lower precedence tasks. For many tasks, static prioritization is not necessary or even appropriate because tasks can often be achieved in variable ways, as in reaching. In this paper, we show that such task variability can be used to modulate task priorities during execution, to temporarily deviate certain tasks as needed, in the presence of incompatibilities. We first present a method for mapping from task variance to task priority and then provide an approach for computing task variance. Through three common conflict scenarios, we demonstrate that mapping from task variance to priorities reactively solves a number of task incompatibilities.

This work was presented at the international conference on intelligent robots and systems [2].

Task compatibility optimization. Highly redundant robots, such as humanoids, can execute multiple simultaneous tasks allowing them to perform complex whole-body behaviors. Unfortunately, tasks are generally planned without close consideration for the underlying controller being used, or the other tasks being executed. Because of this, tasks are often incompatible with one another and/or the system constraints, and cannot always be accomplished simultaneously. These incompatibilities can be managed using prioritization and gains, but tuning them is tedious. In this work, we take an alternative approach and develop a task compatibility optimization loop which automatically improves task compatibility by modifying their trajectories using reinforcement learning. To do so, the tasks are iteratively optimized by minimizing a compatibility cost, which measures the compatibility between one or more tasks, and the system constraints. Using two common scenarios, we show that task compatibility optimization results in whole-body behaviors which better match the original intent of the task combination without the need for manual tuning of task/controller parameters, heuristics, or re-planning.

This work was submitted for presentation at a robotics journal [3].

Chapter 3

Learning soft task priorities for control of redundant robots (INRIA & TUDA)

Learning soft task priorities for control of redundant robots

Valerio Modugno[1,4], Gerard Neumann[2], Elmar Rueckert[2], Giuseppe Oriolo[1], Jan Peters[2,3], Serena Ivaldi[2,4]

***Abstract*— One of the key problems in planning and control of redundant robots is the fast generation of controls when multiple tasks and constraints need to be satisfied. In the literature, this problem is classically solved by multi-task prioritized approaches, where the priority of each task is determined by a weight function, describing the task strict/soft priority. In this paper, we propose to leverage machine learning techniques to learn the temporal profiles of the task priorities, represented as parametrized weight functions: we automatically determine their parameters through a stochastic optimization procedure. We show the effectiveness of the proposed method on a simulated 7 DOF Kuka LWR and both a simulated and a real Kinova Jaco arm. We compare the performance of our approach to a state-of-the-art method based on soft task prioritization, where the task weights are typically hand-tuned.**

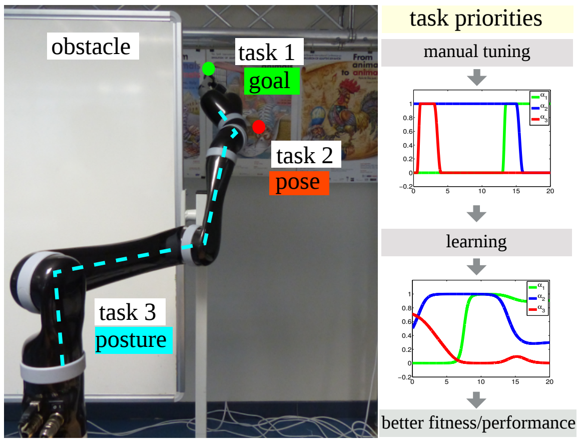

Fig. 1. The Jaco arm must reach a goal behind a wall (obstacle) while fulfilling a pose task on joint 4 and a full posture task. The initial sequencing of task priorities is not efficient. Our method allows the automatic learning of the temporal profiles of the task priorities from scratch.

I. Introduction

Exploiting the redundancy in robotic systems to simultaneously fulfil a set of tasks is a classical problem for complex manipulators and humanoid robots [1], [2]. Several controllers have been proposed in the literature, where the tasks combination is determined by the relative importance of the tasks, expressed by the task priorities. There are two main approaches for prioritized multi-task controllers. The first is based on *strict task priorities*, where a hierarchical ordering of the tasks is defined: critical tasks (or tasks that are considered as more important) are fulfilled with higher priorities, and the low-priority tasks are solved in the null-space of the higher priority tasks [3], [4]. The second is based on *soft task priorities*, where the solution is typically given by a combination of weighted tasks [5]. The importance or "soft priority" of each individual task is represented by a scalar weight function, which evolves in time depending on the sequencing of the robot actions. By tuning the time-dependent vector of scalar weights, the global robot motion can be optimized. In simulation studies, it was shown that adapting these weights may result in a seamless transition between tasks (*i.e.*, reaching for an object, staying close to a resting posture and avoiding an obstacle), as well as in continuous task sequencing [6].

When complex robots, such as humanoids, need to perform manipulations while fulfilling many tasks and constraints (*e.g.*, tracking a desired trajectory, avoiding obstacles, controlling the interaction forces), the strict task priorities approaches typically require a priori a definition of the task hierarchy. For instance, Sentis and Khatib [7] defined three levels of hard priorities *i.e.*, constraints of utter importance (such as contacts, near-body objects, joint-limits and self-collisions), operational tasks demands (*i.e.*, manipulation and locomotion) and adaptable postures (*i.e.*, the residual motion). However, in many contexts, it is difficult to organize the tasks in a stack and pre-define their relative importance in forms of priorities. When priorities are strict, a higher-priority task can completely block lower-priority tasks, which can result in movements that are not satisfactory for the robot mission (*i.e.*, its "global" task). Another issue concerns the occurrence of discontinuities in the control law due to sudden changes in the prioritization [8].

Soft task priorities provide an appealing alternative solution. However, the simultaneous execution of different elementary tasks with variable soft priorities can lead to incompatibilities that might generate undesired movements or prevent the execution of some tasks. These issues are well explained in [9], where the authors modulate the task weights based on the movement variance to handle incompatibilities during online execution. Finally, when the number of tasks increases, for example in whole-body control of humanoid robots, and some tasks related to safety (*e.g.*, balance) are given high priority, it is generally difficult to define suitable task activations. In this case the priorities and their transitions are manually tuned by expert users [10] or defined before-hand [11]. Among the methods based on

*This paper was supported by the FP7 EU projects CoDyCo (No. 600716 ICT 2011.2.1 Cognitive Systems and Robotics).

[1] Dipartimento di Ingegneria Informatica, Automatica e Gestionale, Sapienza Universita di Roma, via Ariosto 25, 00185 Roma, Italy. modugno@diag.uniroma1.it

[2] Intelligent Autonomous Systems Lab., TU Darmstadt, Germany.

[3] Max Planck Institute for Intelligent Systems.

[4] Inria, Villers-lès-Nancy, F-54600, France; CNRS, Loria, UMR n.7503 and Université de Lorraine, Loria, UMR n.7503, Vandoeuvre-lès-Nancy, F-54500, France. serena.ivaldi@inria.fr

soft priorities, recently Liu et al. [6] proposed a generalized projector (GHC) that handles strict and non-strict priorities with smooth transitions when tasks priorities are swapped. Despite the elegant framework, their controller needs again a lot of manual tuning. The evolution of the tasks priorities in time, the timing and the tasks transitions need to be designed by hand. While this approach could still be easy for few tasks and simple robotic arms, it quickly becomes unfeasible for complex robots such as humanoids performing whole-body movements that usually require a dozen of tasks and constraints (*e.g.*, control balance, posture, end-effectors, stabilize head gaze, prevent slipping, control the interaction forces *etc.*). With the increasing abilities of humanoid robots, the number of tasks increases, together with their weights or priorities: their manual tuning through a sequence of complex manipulations becomes a major bottleneck.

In this paper, we propose a framework that addresses the issue of automatically optimising the task priorities by means of a learning algorithm. The proposed concept of learning the soft priorities can be applied to existing multi-task frameworks, such as the GHC [10]. However, we use here a simpler controller based on a regularized version of the Unified Framework for Robot Control (UF) [13] proposed by Peters *et al.* In our framework, the task weight functions are parametrized functional approximators that can be automatically learned by state-of-the-art stochastic optimization algorithms. The *temporal* profiles of the task weights can be learned by optimizing a given fitness function, used to evaluate the performance of candidate task priorities. In contrast to many cost functions used in whole-body optimisation frameworks, here we do not require the fitness to be a linear or quadratic function.

We show the effectiveness of our approach on both a simulated and a real 6 degrees of freedom (DOF) Kinova Jaco arm, on a goal reaching problem with several elementary tasks. Furthermore, we compare the performance of our controller with the state-of-the-art method GHC proposed by Liu *et al.* [10] on a simulated 7 DOF Kuka LWR arm.

The paper is organized as follows. Section II presents the proposed approach, describing the structure of the controllers, the task weight functions and the learning procedure. We present the experimental results in Section III, draw conclusions and discuss future work in Section IV.

II. Methods

Let us consider a "global task" or a "mission" for a redundant robot: for example, *to reach a goal point behind a wall while avoiding an obstacle*. The overall movement can be entirely planned by exploring all the possible joint configurations, or it can be generated by a combination of a set of controllers solving simpler elementary tasks (for example: control the end-effector, control the pose of a particular link, *etc.*). We assume that the set of elementary tasks is known, and that each task can be executed by a given torque controller. The global movement can be evaluated by a fitness function ϕ that can be used as a measure of the ability of the robot to fulfil its mission. Our method aims at automatically learning the task priorities (or task weight functions) to maximize the robot performance.

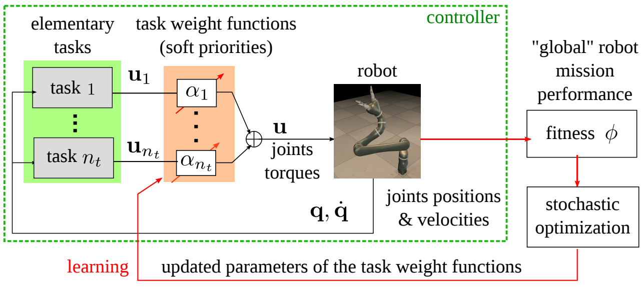

controller
elementary tasks
task weight functions (soft priorities)
task 1
$\mathbf{u}_1$
α_1
task n_t
$\mathbf{u}_{n_t}$
α_{n_t}
$\mathbf{u}$
joints torques
robot
"global" robot mission performance
fitness ϕ
stochastic optimization
$\mathbf{q}, \dot{\mathbf{q}}$
joints positions & velocities
learning
updated parameters of the task weight functions

Fig. 2. Overview of the proposed method. The controller consists of a weighted combination of elementary tasks, where the weight functions represent the soft task priorities. An outer learning loop enables the optimization of the task weights parameters.

An overview of the proposed approach is illustrated in Fig. 2. In Section II-A we describe the controller $\mathbf{u}_i$ for each elementary task: a regularized version of the Unified Framework [13]. In Section II-B we describe the multi-task controller with learned task priorities. In Section II-C we describe the parametrized task weight functions α_i used by our multi-task controller, and discuss the parameters optimization. As a learning algorithm, we propose the Covariance Matrix Adaptation Evolution Strategy (CMA-ES) [14], a derivative-free stochastic optimization algorithm, in view of its good exploration properties and ease of use.

A. Controller for a single elementary task

We hereby describe the torque controller for the i-th elementary task. To simplify the controller design, we decided to adopt the Unified Framework (UF) [13]. We consider the well-known rigid-body dynamics of a robot with n DOF, *i.e.*,

$$\mathbf{M}(\mathbf{q})\ddot{\mathbf{q}} + \mathbf{f}(\mathbf{q},\dot{\mathbf{q}}) = \mathbf{u}_i(\mathbf{q},\dot{\mathbf{q}}), \tag{1}$$

where $\mathbf{q}$, $\dot{\mathbf{q}}$, $\ddot{\mathbf{q}} \in \mathbb{R}^n$ are, respectively, the joints positions, velocities and accelerations, $\mathbf{M}(\mathbf{q}) \in \mathbb{R}^{n\times n}$ is the generalized inertia matrix, $\mathbf{f}(\mathbf{q},\dot{\mathbf{q}}) \in \mathbb{R}^n$ accounts for Coriolis, centrifugal and gravitational forces and $\mathbf{u}_i(\mathbf{q},\dot{\mathbf{q}}) \in \mathbb{R}^n$ is the vector of the commanded torques of the i-th task. Using the same notation as in [13], we describe the task as a constraint, given by $\mathbf{h}_i(\mathbf{q},\dot{\mathbf{q}},t) = \mathbf{0}$, where $\mathbf{h}_i \in \mathbb{R}^m$ is at least a twice differentiable function, where m is the task dimension. By differentiating the constraint with respect to time, we obtain:

$$\mathbf{A}_i(\mathbf{q},\dot{\mathbf{q}},t)\ddot{\mathbf{q}} = \mathbf{b}_i(\mathbf{q},\dot{\mathbf{q}},t), \tag{2}$$

where $\mathbf{A}_i(\mathbf{q},\dot{\mathbf{q}},t)$ is a known $m\times n$ matrix and $\mathbf{b}_i(\mathbf{q},\dot{\mathbf{q}},t)$ is a $m\times 1$ vector. For example, given a simple tracking control task with $\mathbf{h}_i(\mathbf{q},\dot{\mathbf{q}},t) = \mathbf{q} - \mathbf{q}^{des}$, where $\mathbf{q}^{des}$ corresponds to a desired trajectory. By computing the second order derivative in t we obtain $\ddot{\mathbf{q}} = \ddot{\mathbf{q}}^{des}$, where $\mathbf{b} = \ddot{\mathbf{q}}^{des}$ and $\mathbf{A}_i = \mathbf{I}$ (with $\mathbf{I}$ the identity matrix). Applying Gauss's principle, it is possible to derive a controller that fulfils the constraints by minimizing the cost function $\zeta_i(t) = \mathbf{u}_i^\top \mathbf{N}_i(t)\mathbf{u}_i$, where $\mathbf{N}_i(t)$ is a positive semidefinite matrix. The optimization problem is defined by

$$\mathbf{u}_i^* = \arg\min_{\mathbf{u}_i} \zeta_i(t) = \arg\min_{\mathbf{u}_i} \left[\mathbf{u}_i^\top \mathbf{N}_i(t)\mathbf{u}_i\right], \tag{3}$$

subject to Eq. 1 and 2. The solution to this optimization problem is given by

$$\mathbf{u}_i = \mathbf{N}_i^{-\frac{1}{2}}(\mathbf{A}_i\mathbf{M}^{-1}\mathbf{N}_i^{-\frac{1}{2}})^{\#}(\mathbf{b}_i + \mathbf{A}_i\mathbf{M}^{-1}\mathbf{f}), \tag{4}$$

where $(\cdot)^{\#}$ is the Moore-Penrose pseudoinverse and the upper script in $\mathbf{N}_i^{-\frac{1}{2}}$ denotes the inverse of the matrix square root. Controllers derived from UF are sensitive to kinematic singularities, due to the matrix inversion [15]. To overcome this problem, we reformulate the UF controller in a *regularized* fashion, as classically done at the kinematic level, for instance in [16]. The objective function of UF can be reformulated in such a way that the solutions of the optimization problem naturally exhibit a damped least squares structure (at the price of a loss of precision in the execution of the elementary task). Given the dynamical model of the robot (Eq. 1) and the constraint that describes the task (Eq. 2), we define the regularized optimal control problem:

$$\underset{\mathbf{u}_i}{\arg\min}\, \zeta_i(t) = \underset{\mathbf{u}_i}{\arg\min}\left[(\mathbf{A}_i\ddot{\mathbf{q}} - \mathbf{b}_i)^2 + \mathbf{u}_i^{\top}\frac{\mathbf{N}_i(t)}{\lambda_i}\mathbf{u}_i\right], \tag{5}$$

where λ_i is the regularizing factor with a l^2-weighted norm for the regularization term. In the simplest case, λ_i can be a manually-tuned constant value, or automatically determined by more sophisticated methods, as done in [17], based on the smallest singular value of the matrix to invert. To derive the closed form solution of the optimization problem, we substitute $\ddot{\mathbf{q}}$ in Eq. 5 with the expression obtained by solving the dynamical constraint for $\ddot{\mathbf{q}}$. The resulting closed form solution of the controller for a single elementary task is then:

$$\mathbf{u}_i = \mathbf{N}_i^{-1}\tilde{\mathbf{M}}_i^{\top}(\mathbf{I}\lambda_i^{-1} + \tilde{\mathbf{M}}_i\mathbf{N}_i^{-1}\tilde{\mathbf{M}}_i^{\top})^{-1}(\mathbf{b}_i + \tilde{\mathbf{M}}_i\mathbf{f}), \tag{6}$$

with $\tilde{\mathbf{M}}_i = \mathbf{A}_i\mathbf{M}^{-1}$.

B. Controller for multiple elementary tasks with soft task priorities

With reference to the scheme of Fig. 2, we consider a number n_t of elementary tasks, that can be combined by the robot to accomplish a given "global" mission. The solution of the i-th task is provided by the torque controller $\mathbf{u}_i$ described in the previous section. Each task is modulated by a task priority or task weight function $\alpha_i(t)$. The ensemble $\{\alpha_i(t)\}_{i=1,\dots,n_t}$ constitutes the *activation policy* that determines the overall robot movement. The robot controller is therefore given by

$$\mathbf{u}(\mathbf{q},\dot{\mathbf{q}},t) = \sum_{i=1}^{n_t}\alpha_i(t)\,\mathbf{u}_i(\mathbf{q},\dot{\mathbf{q}}) \;, \tag{7}$$

where t is the time, and $\mathbf{q}$ and $\dot{\mathbf{q}}$ are the robot joint positions and velocities. The task priorities $\alpha_i(t)$ are scalar functions and their time profile can be optimized. We automatically tune the task priorities with a learning algorithm. We seek the best task weight functions that maximize a defined performance measure, or fitness, evaluating the execution of the global task. As finding the optimal functions $\alpha_i^*(t)$ is an intractable problem, we turn the functional optimization problem into a numerical optimization problem by representing the task priorities with parametrized functional approximators, $\alpha_i(t) \rightarrow \hat{\alpha}_i(\boldsymbol{\pi}_i,t)$, where $\boldsymbol{\pi}_i$ is the set of parameters that shape the temporal profile of the i-th task weight function. The controller then becomes:

$$\mathbf{u}(\mathbf{q},\dot{\mathbf{q}},t) = \sum_{i=1}^{n_t}\hat{\alpha}_i(\boldsymbol{\pi}_i,t)\,\mathbf{u}_i(\mathbf{q},\dot{\mathbf{q}}) \tag{8}$$

Finding the optimal task priorities consists therefore in finding the optimal parameters $\boldsymbol{\pi}_i^*$, which can be done applying a learning method to maximize the fitness ϕ.

C. Learning the task priorities

We model the task priorities by a weighted sum of normalized Radial Basis Functions (RBF):

$$\hat{\alpha}_i(\boldsymbol{\pi}_i,t) = S\left(\frac{\sum_{k=1}^{n_r}\pi_{ik}\psi_k(\mu_k,\sigma_k,t)}{\sum_{k=1}^{n_r}\psi_k(\mu_k,\sigma_k,t)}\right), \tag{9}$$

where $\psi_k(\mu_k,\sigma_k,t) = \exp\left(-1/2[(t-\mu_k)/\sigma_k]^2\right)$, with (μ_k,σ_k) being mean and variance of the basis functions, n_r is the number of RBFs and $\boldsymbol{\pi}_i = (\pi_{i1},\dots,\pi_{in_r})$ is the set of parameters of each task priority. $S(\cdot)$ is a sigmoid function that squashes the output to the range $[0,1]$. When the task priority is 1, the task is fully activated; when its value is 0, the task is not active.

In our method, learning the task priorities is implemented by learning the free parameters $\boldsymbol{\pi}_i$ of the weight functions (Eq. 9). We optimize the parameters with respect to a known fitness function $\phi = \phi(\mathbf{q}_{t=1,\dots,T},\mathbf{u}_{t=1,\dots,T},t)$, given T time steps. ϕ describes the performance of the controller in fulfilling its global mission. The fitness function could be a simple measure of success in case of goal reaching, the time duration of a movement, the energy consumption *etc.* More criteria for optimizing robot motions in optimal control frameworks are reported in [18]. If the fitness function ϕ is differentiable with respect to the controls and the parameters (which requires the function approximators to be differentiable as well with respect to the controls [17]), then gradient methods can be used. If the fitness is not differentiable with respect to the parameters, then a derivative-free method can be used. Thus, derivative-free methods are appealing, since they do not constrain the design of the fitness function. Furthermore, recent results showed that it is possible to achieve very fast performances in trial-and-error learning with derivative-free methods [19].

As optimization algorithm, we use CMA-ES [14], which is a stochastic derivative-free optimization strategy that is suitable for non-linear and non-convex objective functions. This method belongs to the class of evolutionary algorithms. At each iteration of the algorithm, new candidate solutions are generated from a population of candidates through stochastic sampling. The fitness function is then used to evaluate the candidates. In our case, each candidate is a possible set of parameters for the task priorities $\mathbf{x} = \{\boldsymbol{\pi}_1,\dots,\boldsymbol{\pi}_{n_t}\}$ (Eq. 9). At each iteration of the algorithm (called *generation*), a new population of candidates is generated by sampling a multivariate normal distribution $\mathcal{N}(\mathbf{m},\boldsymbol{\Omega})$, where $\mathbf{m}$ and

$\mathbf{\Omega}$ represent respectively mean and covariance of the distribution. A fitness value is computed for each candidate in the current population and, according to the fitness, only the most promising candidates are kept to update the search distribution. Given the n_c candidates $\{\mathbf{x}_1, \dots, \mathbf{x}_{n_c}\}$, the algorithm selects the $n_b < n_c$ best ones according to their ordered fitness values $\{\hat{\mathbf{x}}_1, \dots, \hat{\mathbf{x}}_{n_b}\}$. It uses the selecte candidates to compute the mean of the sampling distributio at the next iteration: $\mathbf{m}^{(new)} = \sum_{i=1}^{n_b} \omega_i \hat{\mathbf{x}}_i$, with $\sum_{i=1}^{n_b} \omega_i = 1$. Then the covariance matrix is updated as:

$\mathbf{\Omega}^{(new)} = (1 - c_1 - c_2)\mathbf{\Omega} + c_1 p_\Omega p_\Omega^\top + c_2 \sum_{i=1}^{n_b} \omega_i \mathbf{y}_i (\mathbf{y}_i)^\top$ with $\mathbf{y}_i = (\hat{\mathbf{x}}_i - \mathbf{m})$, c_1 and c_2 two predefined parameter (see [14] for more details). The symbol p_Ω is a tern measuring the correlation among successive generations. Th covariance is related to the *exploration rate* of the algorithm a scalar value between [0,1] and the only parameter of th algorithm that needs to be tuned. This version of CMA-E does not support constrained optimization, which means that the optimized solutions that are not physically feasible on the real robot must be dropped and the learning algorithm restarted. In the follow-up of this work, we will use a version that supports constraints [20].

III. Experiments

In this section we discuss our experiments on learning the task priorities. We start showing on a simulated Kinova Jaco arm that the our learning method improves the performance of the movement in terms of fitness values, over existing task priorities that have been manually tuned. We also show that the optimized trajectories are robust with respect to the initialization of the learning process. We compare on a real Jaco arm some typical learned policies with the manually tuned one, showing that our method improves the real robot motion. Finally, we compare on a simulated Kuka LWR the performance of our method with the state-of-art GHC controller [6] . We show that our method is not only better in terms of performance, but also computationally 10 times faster.

A. Learning the task priorities for the Kinova Jaco arm

The setting for the first experiment is shown in Figure 1. The Kinova Jaco arm (6 DOF), starting from its zero configuration, must reach a desired position behind a wall with its end-effector. The goal position is difficult to reach, and the robot kinematics is such that it is not straightforward to manually design a trajectory that does not collide with the obstacle and brings the hand to the goal.

There are 3 given elementary tasks. The first is about reaching the Cartesian position $\mathbf{p}^* =$[0, -0.63, 0.7] with the end-effector (*goal*). The second is about reaching the Cartesian pose [-0.31, -0.47, 0.58] with the 4th link. The third is about keeping the joint configuration [120, 116, 90, 0, 0, 0] (degrees).We design the following fitness function $\phi \in [-1, 0]$:

$$\phi(\mathbf{q}_{1,\dots,T}, \mathbf{u}_{1,\dots,T}) = -\frac{1}{2}\left(\frac{\sum_i^T \|\mathbf{p}_i - \mathbf{p}^*\|}{\varepsilon_{\max}} + \frac{\sum_i^T \|\mathbf{u}_i\|_2^2}{u_{\max}}\right)$$

where T is the number of control steps (the task duration is 20 seconds, and we control at 10ms), $\mathbf{p}_i$ describes the end-effector position at time i and $\mathbf{p}^*$ is the goal position, $\|\cdot\|_2^2$ is the square of the ℓ^2 norm and $\varepsilon_{\max}^{-1}$ and $u_{\max}^{-1}$ are two scaling factors.

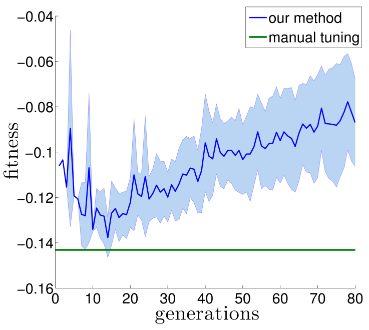

Fig. 3. Average fitness value for the task priorities learned with our method, for the 3-tasks experiment with the simulated Jaco arm. The horizontal line indicates the fitness of the manually tuned solution. The mean and standard deviation of the fitness for the learned policies is computed over 100 restarts of CMA-ES, each with 80 generations and random initialization of the parameters. We only retained the fitness for the experiments that provided solutions satisfying the real robot constraints.

The first term of ϕ penalizes the cumulated distance from the goal that enforces a minimum time transfer trajectory for the robot arm, while the second term penalizes the global control effort. To ensure that the generated controls are feasible for the real Jaco robot, we set the fitness to -1 whenever the generated policy violates one of the robot constraints: a collision with the environment, joints position ranges and maximum joint torques. This ad-hoc solution is also a consequence of the learning algorithm. Fig. 3 shows the average fitness value computed over the eleven optimized trajectories satisfying the constraints, found on 100 restarts of CMA-ES.

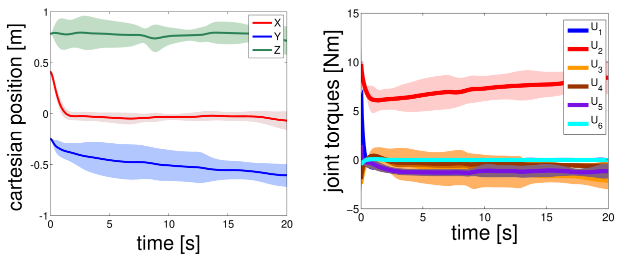

Fig. 4. Mean and variance of the Cartesian trajectory of the end-effector and the joints torques of the simulated Jaco arm, generated by learned task priorities over 100 trials of the 3-tasks experiment (see text in Section III-B). Even starting from random initialization of the task weight parameters, the learning process is eventually able to produce similar optimized motions of the robot that fulfil its 'global' task.

B. Robustness of the learning process

Different profiles of the task priorities can yield similar movements of the robot. It is however important to show that the learning process is able to optimize the task priorities in a robust way, that is providing similar optimal solutions. We therefore execute N=100 replicates of the experiment in Section III-A, with a simulated Jaco arm and three tasks. In each experiment, CMA-ES runs for 100 generations with an exploration rate of 0.5. The parameters are randomly

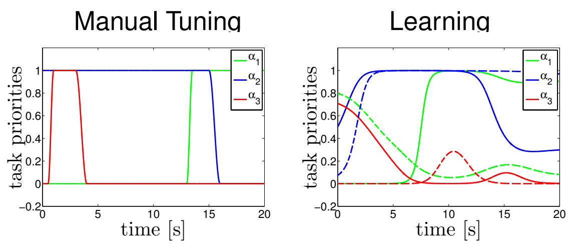

(a) The task priorities evolving in time.

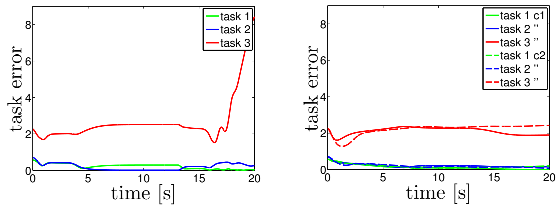

(b) The task errors.

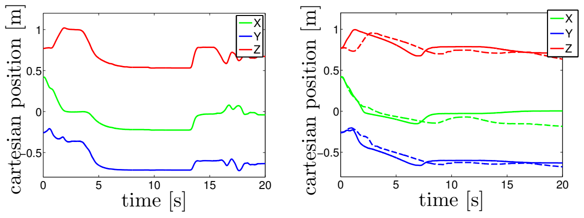

(c) The end-effector trajectory in the Cartesian space.

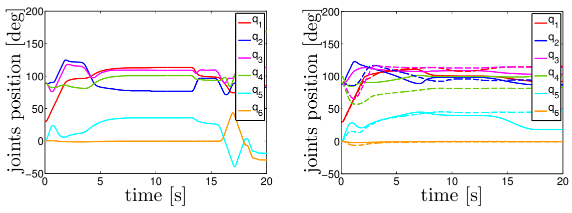

(d) The joints trajectories.

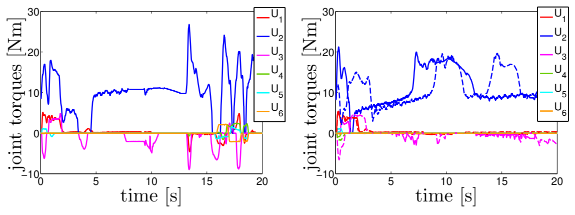

(e) The measured joints torques (estimated by the motor currents).

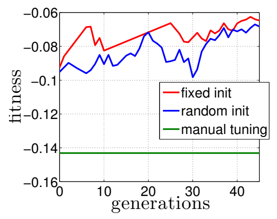

(f) The fitness values.

Fig. 5. Comparison between a manually tuned (left side) and two typical learned (right side) policies for the 3-tasks experiment performed with the real Kinova Jaco arm. On the right, a solid line corresponds to a policy optimized starting from a fixed/known initial value of the priorities (*fixed init*), in this case the priorities found by manual tuning; the dashed line corresponds to a policy optimized starting from random values (*random init*). The final fitness values are: -0.1431 (manual tuning), -0.0585 (fixed init) and -0.0644 (random init).

initialized. We compute the average and standard deviation of the solutions that satisfy the robot and task constraints. Figure 4 shows the average end-effector trajectory in the Cartesian space and the corresponding joint torques. Despite the redundancy of the robot and the one of the task priorities, the final robot movements are smooth and quite consistent with each other. Their average fitness is -0.0874 ± 0.0213. Overall, this result indicates that learning the soft task priorities starting from scratch (*i.e.*, where an initial guess for the activation of the task priorities in time is not available) is a viable and robust option for generating the motion of redundant robots.

C. Experiment on the real Kinova Jaco arm

We compare in Fig. 5 the effect of three different task prioritizations on the real Jaco arm. In the left column, we show the robot movement generated by task priorities that were manually tuned by an expert user of the Kinova arm; on the right column, we show two typical robot movements generated by learned task priorities, which were optimized with CMA-ES starting from a known initial value (the manually tuned task weight functions) and a random value. We set the exploration rate in CMA-ES to 0.5 and perform 40 generations. Learning the priorities has a beneficial effect on the smoothness of the trajectories, which becomes evident when comparing the plots of the end-effector (Fig. 5c), joints positions (Fig. 5d) and torques (Fig. 5e) and the task errors (Fig. 5b). We evaluate the fitness using the commanded joint torques $\mathbf{u}_i$ and the kinematics and dynamics model of the Jaco arm to compute $\mathbf{p}_i$. The fitness value for the manually tuned task priorities is -0.1431. The fitness values for the two optimized solutions are better: -0.0585 and -0.0644 initializing the parameters with fixed and random values respectively. Overall, this experiment illustrates that learning the task priorities improves the real robot motion with respect to an existing manually tuned solution.

D. Comparison with the state-of-the-art GHC

In this experiment we compare the performance of the task priorities learning applied to our method and to the state-of-the-art multi-task controller GHC [6].

In the GHC, each task is associated to a null space projector of the extended Jacobian that contains the analytical description of all the task objectives. Soft task prioritization is achieved because the null space projector depends on a set of manually designed weight functions ranging from 0 to 1, that control if each task is fully or partially projected in the null spaces of the other tasks with higher priority. The controller is the solution to a quadratic optimal control problem subject to the robot and task constraints – see [6]. The soft task priorities are introduced as a further constraints, formulated by $\ddot{\mathbf{q}} = \sum_{i=1}^{n_t} \mathbf{P}_i(\mathbf{\Lambda}_i)\ddot{\mathbf{q}}_i^{'}$, where $\mathbf{P}_i(\cdot)$ is the null space projector associated to the i-th task, $\mathbf{\Lambda}_i$ is a matrix that depends on the task priorities, $\ddot{\mathbf{q}}_i^{'}$ are intermediate joint accelerations associated to each task and $\ddot{\mathbf{q}}$ are the joints accelerations. To enable the comparison with our method,

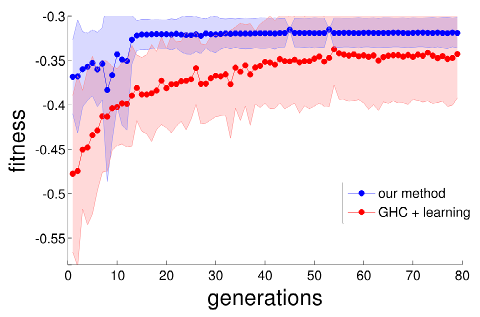

Fig. 6. Comparison between our method and the GHC modified to learn the task priorities with CMA-ES. The plot shows the mean and the standard deviation of the fitness in $R = 20$ trials of the experiment with the simulated KUKA LWR arm (see Section III-D). For both controllers, the learning is initialized with random parameters. Our method shows a faster convergence and better optimization of the fitness. The average fitness is is -0.0373 ± 0.0320 for our method and -0.0735 ± 0.0946 for the GHC+learning. The two distributions are statistically different ($p < 0.01$ with the K-S test).

we parametrized the task priority matrix $\mathbf{\Lambda}_i$ for each task i in the same way as described in Section II-B.

We compare the two methods on a reaching task with a simulated 7 DOF Kuka LWR, which was originally used in [6]. In this scenario, the robot must reach a goal point beneath a rectangular surface parallel to the ground ($z = 0.25m$), without collision. The are 2 elementary tasks. The first is about reaching the Cartesian position $\mathbf{p}^*$ =[0.6, 0, 0.15] with the end-effector (*goal*). The second is about keeping the joint configuration [0, 90, 0, -90, 0, 90, 0] (degrees). We design the following fitness function $\phi \in [-1, 0]$:

$$\phi(\mathbf{q}_{1,\dots,T}, \mathbf{u}_{1,\dots,T}) = -\frac{1}{2}\left(\frac{\sum_i^T \|\mathbf{p}_i - \mathbf{p}^*\|}{\varepsilon_{\max}} + \frac{\max(\|\mathbf{u}_{i=1,\dots,T}\|_\infty)}{u_{\max}}\right)$$

where $\|\cdot\|_\infty$ is the infinity norm. We set the fitness to -1 in case of collision. We run 20 experiments from random initial parameters for both methods, with an exploration rate of 0.1 for CMA-ES and 80 generations.

Our method generated solutions that satisfy the collision constraint in 90% of the cases, while the GHC succeeded only in 75%. Figure 6 shows the mean and standard deviation of the fitness: our method is faster in convergence and improves the final optimized fitness. The average fitness at the end of the learning process is -0.0373 ± 0.0320 for our method and -0.0735 ± 0.0946 for the GHC+learning. The two distributions of the fitness are statistically different ($p = 0.0073 < 0.01$, obtained with the two-sample Kolmogorov-Smirnov test). Our method is also 10 times faster in terms of computational time: on a standard i7 machine, the average time for the optimization process to find a solution with 80 generations (average over 20 trials) is $3.7 \times 10^3 \pm 2.4 \times 10^2$ seconds for our method and $3.9 \times 10^4 \pm 2.2 \times 10^3$ seconds for the GHC+learning approach.

IV. Conclusion and Future Work

In this paper we address an important issue for prioritized multi-task controllers, that is the automatic and optimal generation of task priorities through parametrized weight functions. As a first step towards an automatically tuned controller for redundant robots, we propose a novel framework with a multi-task controller where the task priorities can be learned via stochastic optimization. We show the effectiveness of our approach by comparing to GHC [10], a state-of-the-art multi-task prioritized controller. We present several results performed on a simulated 7 DOF Kuka LWR arm and both a simulated and a real 6 DOF Kinova Jaco arm. Ongoing work is focused on improving the current framework from different points of view: addressing generalization, using constraints inside the optimization, and scaling up the method to handle robots with several DOF, e.g., humanoid robots.

References

[1] Y. Nakamura, H. Hanafusa, and T. Yoshikawa, "Task-priority based redundancy control of robot manipulators," *IJRR*, vol. 6, no. 2, pp. 3–15, 1987.

[2] B. Siciliano and J.-J. Slotine, "A general framework for managing multiple tasks in highly redundant robotic systems," in *Int. Conf. Advanced Robotics*, 1991, pp. 1211–1216.

[3] L. Saab, O. Ramos, F. Keith, N. Mansard, P. Soueres, and J.-Y. Fourquet, "Dynamic whole-body motion generation under rigid contacts and other unilateral constraints," *IEEE Trans. on Robotics*, vol. 29, pp. 346–362, Jan 2013.

[4] A. Del Prete, F. Nori, G. Metta, and L. Natale, "Prioritized motion-force control of constrained fully-actuated robots: Task space inverse dynamics," *Robotics and Autonomous Systems*, vol. 63, pp. 150–157, Jan 2015.

[5] J. Salini, V. Padois, and P. Bidaud, "Synthesis of complex humanoid whole-body behavior: A focus on sequencing and tasks transitions," in *ICRA*, 2011, pp. 1283–1290.

[6] M. Liu, Y. Tan, and V. Padois, "Generalized hierarchical control," *Autonomous Robots*, pp. 1–15, 2015.

[7] L. Sentis and O. Khatib, "Synthesis of whole body behaviours through hierarchical control of behavioral primitives," *Int. Journal of Humanoid Robotics*, pp. 505–518, 2005.

[8] C. Ott, A. Dietrich, and A. Albu-Schffer, "Prioritized multi-task compliance control of redundant manipulators," *Automatica*, vol. 53, pp. 416 – 423, 2015.

[9] R. Lober, V. Padois, and O. Sigaud, "Variance modulated task prioritization in whole-body control," in *IROS*, 2015, pp. 1–6.

[10] M. Liu, S. Hak, and V. Padois, "Generalized projector for task priority transitions during hierarchical control," in *ICRA*, 2015, pp. 768–773.

[11] S.-I. An and D. Lee, "Prioritized inverse kinematics with multiple task definitions," *ICRA*, pp. 1423–1430, 2015.

[12] J. Kober, D. Bagnell, and J. Peters, "Reinforcement learning in robotics: A survey," *IJRR*, vol. 11, pp. 1238–1274, 2013.

[13] J. Peters, M. Mistry, F. Udwadia, J. Nakanishi, and S. Schaal, "A unifying framework for robot control with redundant dofs," *Autonomous Robots*, vol. 24, pp. 1–12, Jan 2008.

[14] N. Hansen and A. Ostermeier, "Completely derandomized self-adaptation in evolution strategies." *Evolutionary Computation*, vol. 9, pp. 159–195, Jan 2001.

[15] S. Chiaverini, B. Siciliano, and O. Egeland, "Redundancy resolution for the human-arm-like manipulator," *Robotics and Autonomous Systems*, vol. 8(3), pp. 239–250, Jan 1991.

[16] Y. Nakamura and H. Hanafusa, "Inverse kinematic solutions with singularity robustness for robot manipulator control," *J. Dyn. Sys., Meas., Control*, vol. 108 (3), pp. 163–171, 1986.

[17] S. Ivaldi, M. Fumagalli, F. Nori, M. Baglietto, G. Metta, and G. Sandini, "Approximate optimal control for reaching and trajectory planning in a humanoid robot," in *IROS*, 2010, pp. 1290–1296.

[18] S. Ivaldi, O. Sigaud, B. Berret, and F. Nori, "From humans to humanoids: the optimal control framework," *Paladyn Journal of Behavioral Robotics*, vol. 3, no. 2, pp. 75–91, 2012.

[19] A. Cully, J. Clune, D. Tarapore, and J.-B. Mouret, "Robots that can adapt like animals," *Nature*, vol. 521, no. 7553, pp. 503–507, 2015.

[20] D. V. Arnold and N. Hansen, "A (1+ 1)-cma-es for constrained optimisation," in *GECCO*, 2012, pp. 297–304.

Chapter 4

Learning soft task priorities for safe control of humanoid robots with constrained stochastic optimization (INRIA)

Learning soft task priorities for safe control of humanoid robots with constrained stochastic optimization

Valerio Modugno[1,2], Ugo Chervet[2], Giuseppe Oriolo[1], Serena Ivaldi[2]

***Abstract*— Multi-task prioritized controllers are able to generate complex robot behaviors that concurrently satisfy several tasks and constraints. To perform, they often require a human expert to define the evolution of the task priorities in time. In a previous paper [1] we proposed a framework to automatically learn the task priorities using a stochastic optimization algorithm (CMA-ES), maximizing the robot performance for a certain behavior. Here, we learn the task priorities that maximize the robot performance, ensuring that the optimized priorities lead to safe behaviors that never violate any of the robot and problem constraints. We compare three constrained variants of CMA-ES on several benchmarks, among which two are new robotics benchmarks of our design using the KUKA LWR. We retain (1+1)-CMA-ES with covariance constrained adaptation [2] as the best candidate to solve our problems, and we show its effectiveness on two whole-body experiments with the iCub humanoid robot.**

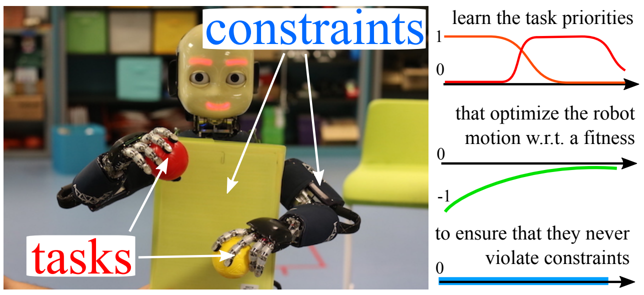
constraints
tasks
learn the task priorities
1
0
that optimize the robot motion w.r.t. a fitness
0
-1
to ensure that they never violate constraints
0

Fig. 1. The humanoid robot iCub performing a bimanual task with several tasks and constraints. In this paper we optimize the task priorities guaranteeing that the global robot behavior is safe: it never violates any of the constraints.

I. Introduction

Fulfilling multiple operational tasks to achieve a complex behavior while satisfying constraints is one of the challenges of whole-body control of redundant manipulators and humanoid robots. For example, let us consider the humanoid iCub (Fig.1) that must fulfil a "global task" *by reaching its hands towards two goal positions behind a wall while avoiding collisions*. The global task can be decomposed as a combination of simpler elementary tasks (for example: control the end-effector, control the pose of a particular link, *etc.*) and constraints that guarantee a condition of feasibility over the generated motions (for example: torque and joint limits, collisions, external forces *etc.*).

More generally, elementary tasks can include tracking desired trajectories, regulating contact forces, controlling the center of mass for balancing *etc*. Constraints range from mechanical limitations (*e.g.*, joint and torque limits) to safety specifications (*e.g.*, collision avoidance, limiting the exchange of mechanical forces with the environment) and balance keeping for floating base platforms.

In the literature, this constrained control problem is usually solved with prioritized controllers, where a set of operational tasks are organized according to strict priorities in a hierarchy or "stack" [3], [4], or combined with weighting functions, also known as soft task priorities [5], [6]. Constraints are either formulated as high-priority tasks or taken into account by quadratic programming solvers. The task priorities and their evolution in time are usually defined *a priori* and frequently manually tuned by experts.

A new line of research is now focused on the automatic optimization of task priorities [1], [7], [8], [9]. Most of these approaches are based on an iterative policy learning technique that needs many repetitions (rollouts) of the same experiment to find a viable solution. These frameworks poorly address the problem of constraints satisfaction when optimizing the task priorities. For example, in [7], torques are saturated for safety, and joint and velocity limits are introduced as tasks. However, satisfaction of constraints formulated as tasks cannot be ensured, especially in the case of soft tasks prioritization. In [8] the balance constraint is added as an objective to the fitness function, but this is a relaxation of the constraint that does not ensure its satisfaction either. In [1] we used the Covariance Matrix Adaptation-Evolutionary Strategy (CMA-ES) [10], a derivative-free stochastic optimization method that solves non-linear, non-differentiable optimization problems, with death penalties to enforce constraint satisfaction on the solutions. This choice was not efficient in terms of searching for the optimum solution, since the exploration could easily get stuck in a constrained region where the fitness landscape was turned into a plateau. Furthermore, many solutions had to be dropped because of constraints violation.

Ensuring that the optimization process yields a safe solution — where safety means not violating any constraints — becomes mandatory if we want to successfully apply these solutions to a real robot [11].

To approach the safety issue, in this paper we investigate *constrained* stochastic optimization algorithms, and we focus on three variants of CMA-ES: one with *vanilla* constraints,

*This paper was supported by the EU FP7 project CoDyCo (n.600716) and by the EU H2020 project COMANOID (n.645097).

[1] Dipartimento di Ingegneria Informatica, Automatica e Gestionale, Sapienza Universita di Roma, via Ariosto 25, 00185 Roma, Italy. modugno@diag.uniroma1.it

[2] Inria, Villers-lès-Nancy, F-54600, France; CNRS, Loria, UMR n.7503 and Université de Lorraine. serena.ivaldi@inria.fr

The authors would like to thank the anonymous reviewers.

one with adaptive constraints [12] and the (1+1)-CMA-ES with covariance constrained adaptation [2]. We compare these methods with a baseline constrained optimization algorithm, (the *fmincon* function in Matlab). To compare the algorithms, we explicitly look for methods that can find good solutions while ensuring zero constraint violations within a reasonable computation time.

There exist standard benchmarks for constrained optimization, consisting in analytic problems with several variables and constraints and known optimal solutions. For example Arnold & Hansen [2] tested (1+1)-CMA-ES on seven different problems with a number of variables ranging from 2 to 10, and a number of constraints between 1 to 9. However, in robotics the number of constraints usually grows with the number of degrees of freedom (DOF) of the robot: for example, with a 7-DOF robot, the joint position range (7×2) and the torque limits (7×2) already introduce 28 constraints. In humanoids and highly articulated systems, the number of DOF is higher (*e.g.*, 32 DOF for the iCub) and so is the number of constraints. Furthermore, the number of tasks increases with the complexity of the action, especially for bimanual or whole-body movements. It is therefore necessary to design new benchmarks tailored for robotics applications to make a pondered decision about the algorithm that is most suited to solve our problem while ensuring that the constraints are never violated.

The contribution of this paper is twofold: first, we compare the performance of three constrained variants of CMA-ES with *fmincon* on analytic and robotic benchmarks, the latter (RB1,RB2) being new and designed *ad hoc*; second, we extend the framework for learning task priorities, which we proposed in [1], to ensure that the optimized priorities lead to safe behaviours that never violate the constraints. We show the effectiveness of our approach by generating optimized and safe (zero constraints violations) whole-body movements on the humanoid robot iCub.

The paper is organized as follows: Section II outlines the framework for learning task priorities for controlling redundant robots; Section III describes the constrained optimization algorithms retained for the study; Section IV and V illustrate the benchmarks comparison and the experiments with the iCub humanoid robot respectively.

II. Multitask controller with learnt priorities

Our method aims at automatically learning the task priorities (or task weight functions) to maximize the robot performance ensuring that the optimized priorities lead to behaviours that always satisfy the constraints. The global robot movement is evaluated by a fitness function ϕ that is used as a measure of the ability of the robot to fulfil its mission without violating the constraints. Our proposed method outlined in Fig. 2 extends the framework that was introduced in [1]. In this section we recall the multi-tasks controller and the structure of the parametrized task weight functions α_i, while the optimization procedure is described in Section III, where we analyze some recent extensions of the basic CMA-ES method that deal with constraints.

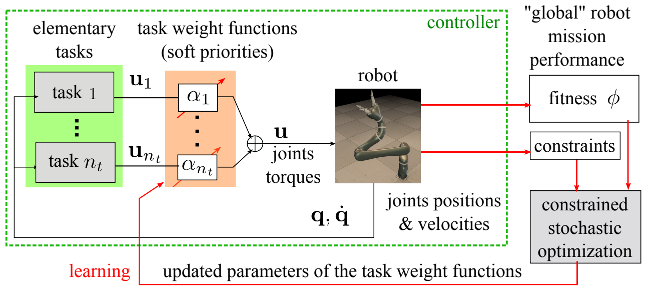

elementary tasks
task weight functions (soft priorities)
controller
"global" robot mission performance
task 1
task n_t
$\mathbf{u}_1$
$\mathbf{u}_{n_t}$
α_1
α_{n_t}
$\mathbf{u}$
joints torques
robot
fitness ϕ
constraints
constrained stochastic optimization
joints positions & velocities
$\mathbf{q}, \dot{\mathbf{q}}$
learning
updated parameters of the task weight functions

Fig. 2. Overview of the proposed method. The controller consists of a weighted combination of elementary tasks, where the weight functions represent the soft task priorities. An outer learning loop enables the optimization of the task weight parameters, taking into account the constraint violations in an explicit way.

A. Controller for a single elementary task

Here, we briefly describe the torque controller for the i-th elementary task, which is presented in more detail in [1]. Following our previous work, we use a regularized closed-form solution of a controller derived from the Unified Framework (UF) [13]. Let us consider the rigid-body dynamics of a robot with n DOF, *i.e.*:

$$\mathbf{M}(\mathbf{q})\ddot{\mathbf{q}} + \mathbf{f}(\mathbf{q},\dot{\mathbf{q}}) = \mathbf{u}_i(\mathbf{q},\dot{\mathbf{q}})$$

where $\mathbf{q}$, $\dot{\mathbf{q}}$, $\ddot{\mathbf{q}} \in \mathbb{R}^n$ are, respectively, the joints positions, velocities, and accelerations; $\mathbf{M}(\mathbf{q}) \in \mathbb{R}^{n\times n}$ is the generalized inertia matrix, $\mathbf{f}(\mathbf{q},\dot{\mathbf{q}}) \in \mathbb{R}^n$ accounts for Coriolis, centrifugal and gravitational forces; and $\mathbf{u}_i(\mathbf{q},\dot{\mathbf{q}}) \in \mathbb{R}^n$ is the vector of the commanded torques of the i-th task. Following the UF formulation, the general torque controller is $\mathbf{u}_i = \mathbf{N}_i^{-\frac{1}{2}}(\mathbf{A}_i\mathbf{M}^{-1}\mathbf{N}_i^{-\frac{1}{2}})^{\dagger}(\mathbf{b}_i + \mathbf{A}_i\mathbf{M}^{-1}\mathbf{f})$, where the matrix $\mathbf{A}_i(\mathbf{q},\dot{\mathbf{q}},t) \in \mathbb{R}^{m\times n}$ and the vector $\mathbf{b}_i(\mathbf{q},\dot{\mathbf{q}},t) \in \mathbb{R}^{m\times 1}$ incorporate the information about the m-dimensional task; $\mathbf{N}_i$ is a weighting matrix that can be changed to achieve different control strategies; $(\cdot)^{\dagger}$ is the Moore-Penrose pseudoinverse; and the upper script in $\mathbf{N}_i^{-1/2}$ denotes the inverse of the matrix square root. Controllers derived from UF are sensitive to kinematic singularities, due to the matrix inversion [14]. To overcome this problem, we reformulate the UF controller in a *regularized* fashion, as classically done at the kinematic level, for instance in [15]. The resulting closed-form solution of the controller for a single elementary task is then: $\mathbf{u}_i = \mathbf{N}_i^{-1}\tilde{\mathbf{M}}_i^{\top}(\mathbf{I}\lambda_i^{-1} + \tilde{\mathbf{M}}_i\mathbf{N}_i^{-1}\tilde{\mathbf{M}}_i^{\top})^{-1}(\mathbf{b}_i + \tilde{\mathbf{M}}_i\mathbf{f})$, with $\tilde{\mathbf{M}}_i = \mathbf{A}_i\mathbf{M}^{-1}$. λ_i is a regularizing factor (we refer to [1] for a more accurate description of the regularization problem leading to this closed-form solution).

B. Controller for multiple elementary tasks with soft task priorities

Each elementary task is modulated by a task priority or task weight function $\alpha_i(t)$. To automatically find the optimal n_t task priorities $\{\alpha_i(t)\}_{i=1,\dots,n_t}$, we transform the functional optimization problem into a numerical optimization problem by representing the task priorities with parametrized functional approximators $\alpha_i(t) \rightarrow \hat{\alpha}_i(\hat{\boldsymbol{\pi}}_i,t)$, where $\hat{\boldsymbol{\pi}}_i$ is the set of parameters that shape the temporal profile of the i-th task weight function. Following the scheme of Fig. 2, given n_t elementary tasks the final controller is given by:

$$\mathbf{u}(\mathbf{q},\dot{\mathbf{q}},t) = \sum_{i=1}^{n_t} \hat{\alpha}_i(\hat{\boldsymbol{\pi}}_i,t)\,\mathbf{u}_i(\mathbf{q},\dot{\mathbf{q}}) \ . \quad (1)$$

C. Learning the task priorities

We model the task priorities as a weighted sum of normalized Radial Basis Functions (RBFs):

$$\hat{\alpha}_i(\hat{\boldsymbol{\pi}}_i,t) = S\left(\frac{\sum_{k=1}^{n_r} \hat{\pi}_{ik}\psi_k(\mu_k,\sigma_k,t)}{\sum_{k=1}^{n_r} \psi_k(\mu_k,\sigma_k,t)}\right), \quad (2)$$

where $\psi_k(\mu_k,\sigma_k,t) = \exp\left(-1/2[(t-\mu_k)/\sigma_k]^2\right)$, with fixed mean μ_k and variance σ_k of the basis functions, n_r is the number of RBFs and $\hat{\boldsymbol{\pi}}_i = (\hat{\pi}_{i1},\ldots,\hat{\pi}_{in_r}) \subseteq \mathbb{R}^{n_P}$ is the set of parameters for each task priority. $S(\cdot)$ is a sigmoid function that squashes the output to the range $[0,1]$. The elementary task is fully activated when the task priority is equal to 1, otherwise the control action fades out until a full deactivation occurs when the priority goes to 0. The free parameters $\hat{\boldsymbol{\pi}}_i$ of each task weight function (Eq. 2) constitute the current parameters set to optimize: $\boldsymbol{\pi} = (\hat{\boldsymbol{\pi}}_1,\ldots,\hat{\boldsymbol{\pi}}_{n_t})$.

To optimize the free parameters $\boldsymbol{\pi}$, we introduce two elements, the fitness function ϕ and the set of inequality and equality constraints g,h:

- the fitness function $\phi = \phi(\mathbf{q}_{t=1,\ldots,T},\mathbf{u}_{t=1,\ldots,T},t)$ computes a performance measure of the global task executed by the robot over T time steps with the current parameters $\boldsymbol{\pi}$. The fitness function can contain different criteria ranging from energy consumption arguments to specific properties of the desired trajectories (*e.g.* speed and smoothness).
- the constraints g,h determine the admissible controls to be applied to the robot. They can be dependent on the robot structure (*e.g.* maximum joint torques and joint ranges), on the environment (*e.g.* obstacles and collisions), on the tasks (*e.g.* safety limits and couplings), *etc.*

The objective of the next section is to formalize the problem of optimizing the parameters $\boldsymbol{\pi}$ that maximize the fitness ϕ, ensuring that the constraints g,h are satisfied.

III. Constrained black-box optimization of task parameters

Learning the parameters $\boldsymbol{\pi} \in \boldsymbol{\Pi} \subseteq \mathbb{R}^{n_P}$ is a constrained optimization problem, as we need to find the optimal parameters $\boldsymbol{\pi}^\circ$ that maximize the objective function $J(\boldsymbol{\pi}) : \mathbb{R}^{n_P} \to \mathbb{R}$ (by default, equivalent to the fitness ϕ):

$$\boldsymbol{\pi}^\circ = \arg\max_{\boldsymbol{\pi}} J(\boldsymbol{\pi})$$

under the inequality and equality constraints g,h:

$$g_i(\boldsymbol{\pi}) \leq 0, i=1,\ldots,n_{IC}; \quad h_j(\boldsymbol{\pi}) = 0, j=1,\ldots,n_{EC} \ .$$

Following our approach in [1], we do not constrain the fitness structure nor its differentiability properties, hence we keep solving the problem with derivative-free methods. In [1] we used CMA-ES [10] for the known advantage of having to tune few parameters. To find feasible solutions that satisfy the constraints, we adopted a death penalty approach. This was clearly not efficient; the constant penalty applied to the fitness has a pathological effect on the exploration of the algorithm, possibly causing the search to get stuck in infeasible regions.

In this paper, we adopt a different strategy and look explicitly for variants of CMA-ES that take into account the constraints in the exploration procedure. Our goals are: 1) to improve the efficiency of the optimization procedure exploiting the constraint information, and 2) to guarantee that every solution found by the stochastic optimization process lies in a region of the parameter space that satisfies all the constraints. Interestingly, we are not interested in algorithms that permit constraints relaxation (hence violation) to find a solution: this is typically the case of real-time quadratic solvers (*e.g.* quadprog and qpOASES).

Among the multitude of constrained black-box optimization algorithms, we focused on three variants of CMA-ES: a *vanilla penalty* CMA-ES, the CMA-ES with *adaptive penalty* approach proposed in [12] and the (1+1)-CMA-ES with *covariance constrained adaptation* proposed in [2]. The first is a baseline CMA-ES that applies a penalty to the fitness that is proportional to the constraint violation. The second method is similar in principle, but the penalty weights are changed following a heuristic that depends on the constraint violation The third does not rely on penalties but updates the covariance whenever a constraint is violated, to drive the exploration away from infeasible regions.

In the rest of this section, we outline the three methods explaining their differences with respect to CMA-ES. In the presentation, we will use the following symbols:

- $J(\cdot)$: objective function
- n_{IC}: number of inequality constraints $g_i(\cdot)$
- n_{EC}: number of equality constraints $h_i(\cdot)$
- $n_C = n_{IC} + n_{EC}$: total number of constraints
- $\boldsymbol{\Pi} \subseteq \mathbb{R}^{n_P}$: parameter space
- $\boldsymbol{\pi}_k \in \boldsymbol{\Pi}$: k-th candidate at the current generation
- K: total number of candidates for each generation
- K_e: number of best candidates or *elites*
- $\boldsymbol{\pi}_{1:K_e}$: best candidates of the current generation
- $\mathcal{N}(\bar{\boldsymbol{\pi}},\boldsymbol{\Sigma})$: Gaussian distribution with mean $\bar{\boldsymbol{\pi}}$ and covariance $\boldsymbol{\Sigma}$
- σ^2: step size
- $l(\boldsymbol{\pi}_k)$: penalty factor
- $\hat{J}(\boldsymbol{\pi}_k) = J(\boldsymbol{\pi}_k) + l(\boldsymbol{\pi}_k)$: penalized objective function

A. Stochastic optimization with CMA-ES (no constraints)

A single iteration (called *generation*) of CMA-ES [10] consists of several steps. A set of K samples $\boldsymbol{\pi}_k$ is drawn from a multivariate Gaussian distribution $\mathcal{N}(\bar{\boldsymbol{\pi}},\sigma^2\boldsymbol{\Sigma})$ with a σ^2 step size; for each sample $\boldsymbol{\pi}_k$ we perform the evaluation of the objective function J, called *fitness*. The samples are sorted using a ranking procedure based on the fitness and an update of the Gaussian distribution is performed according to the best K_e candidates $\boldsymbol{\pi}_{1:K_e}$, called *elites*.

The update step affects the mean, covariance, and step size of the search distribution $\mathcal{N}(\bar{\boldsymbol{\pi}},\sigma^2\boldsymbol{\Sigma})$. The evolution of the mean is influenced by the probability weights P_k of each elite

```
CMA-ES without constraints
function CMA-ES
    for each $gen = 1,\dots,n_{GENERATIONS}$ do
        for each $k = 1,\dots,K$ do
            $\boldsymbol{\pi}_k \sim \mathcal{N}(\bar{\boldsymbol{\pi}},\sigma^2\boldsymbol{\Sigma})$                ▷ samples
            $J_k = J(\boldsymbol{\pi}_k)$                                ▷ evaluation
        end for
        $\boldsymbol{\pi}_{1:K_e} = \mathrm{SORT}(\boldsymbol{\pi}_{k=1:K}, J_{k=1:K})$                ▷ sorting
        $\bar{\boldsymbol{\pi}}^{new} = \sum_{k=1}^{K_e} P_k\boldsymbol{\pi}_k$ with $\sum_{k=1}^{K_e} P_k = 1$
        $\boldsymbol{\Sigma}^{new} = \mathrm{UPDCOV}(\bar{\boldsymbol{\pi}}^{new}, P_{k=1:K_e})$
        $\sigma^{new} = \mathrm{UPDSIGMA}(\sigma)$
        $\bar{\boldsymbol{\pi}} = \bar{\boldsymbol{\pi}}^{new}$   $\boldsymbol{\Sigma} = \boldsymbol{\Sigma}^{new}$   $\sigma = \sigma^{new}$
    end for
end function
```

Fig. 3. Pseudo-code for the basic CMA-ES without constraints.

candidate. A common choice is $P_k = \ln(0.5(K_e+1)) - \ln(k)$. In CMA-ES, premature convergence is avoided by tuning the step size σ^2. Both σ^2 and $\boldsymbol{\Sigma}$ are updated by combining the information from the last generation and all the previous ones. For the update of the stepsize σ^2 and more detail about the algorithm, we refer the reader to [10]. To initialize CMA-ES the user has to specify the exploration rate, a scalar value between [0,1] that controls the starting value of the covariance matrix. Fig. 3 shows the pseudo-code of the algorithm.

B. CMA-ES with Vanilla Constraints

The *vanilla penalty* functions method relies on adding a penalty term to the fitness of a candidate that depends on the constraints violation of the candidate. The method employs a penalized objective function $\hat{J}(\boldsymbol{\pi}_k) = J(\boldsymbol{\pi}_k) + l(\boldsymbol{\pi}_k)$ with the penalty factor $l(\boldsymbol{\pi}_k)$ defined as:

$$l(\boldsymbol{\pi}_k) = \sum_{i=1}^{n_{IC}} r_i \max(0, g_i(\boldsymbol{\pi}_k))^2 + \sum_{j=1}^{n_{EC}} c_j |h_j(\boldsymbol{\pi}_k)|$$

where r_i and c_i are positive constant values. In Fig. 4 we present a pseudo-code for this variant where we refer to the penalization routine with $\mathrm{PENALTY}(\cdot)$.

C. CMA-ES with Adaptive Constraints

The previous method is by far the simplest and the most intuitive, as it applies a penalty that depends on the candidate $\boldsymbol{\pi}_k$. However, one may want to make the penalty term variable, for example depending on the exploration path.

Collange *et al.* [12] proposed a penalty function approach where a set of adaptive weights are tuned to prevent the search process from getting stuck in a local minima of the penalized fitness function $\hat{J}(\cdot)$. A penalized objective function $\hat{J}(\boldsymbol{\pi}_k)$ is therefore used. The key idea is that the penalty factor $l(\boldsymbol{\pi}_k)$ is built to consider the number of feasible solutions per each generation and the activation of each constraint, determined by a heuristic tuned by a user-defined ε_i. In particular, one assigns $l(\boldsymbol{\pi}_k) = \sum_{i=1}^{n_C} w_i [\gamma_i^+(\boldsymbol{\pi}_k)]^2$, where w_i, $i = 1,\dots,n_C$ is the set of adaptive weights, and $\gamma_i^+(\cdot)$ is the positive part of the so-called *ε-normalized constraint values* γ_i, which are used to identify the active constraints. The ε-normalized constraint values γ_i are defined as:

$$\gamma_i = \begin{cases} [g_i(\boldsymbol{\pi}_k) + \varepsilon_i]/\varepsilon_i & \text{for inequality constraints} \\ |h_i(\boldsymbol{\pi}_k)|/\varepsilon_i & \text{for equality constraints} \end{cases} . \quad (3)$$

The user can tune the definition of the constraint violations and the relaxation of the constraints through the parameters $\varepsilon_i > 0, i = 1,\dots,n_C$. For equality constraints $h_i(\cdot)$, a candidate solution $\boldsymbol{\pi}_k$ is labelled "feasible" if $0 \le \gamma_i \le 1$ and "infeasible" otherwise. For inequality constraints $g_i(\cdot)$, a candidate solution $\boldsymbol{\pi}_k$ is labelled "feasible" if $\gamma_i \le 1$ and "infeasible" otherwise (Fig. 5).

The weights update is driven by the ratio of feasible solutions for all the constraints:

$$r_i^{feas} = \frac{\#\text{ feasible solutions for the } i\text{-th constraint in the curr. generation}}{K}$$

$$\bar{r}_i^{feas} = \text{average of } r_i^{feas} \text{ over the last } n_P + 2 \text{ generation}$$

If all the samples $\boldsymbol{\pi}_k$ with $k = 1,\dots,K$ satisfy the i-th constraint, then $r_i^{feas} = 1$; otherwise $r_i^{feas} < 1$. So $\bar{r}_i^{feas} = 1$ only when all the samples satisfy the i-th constraint for $n_P + 2$ generations. Once this condition is met, the weight w_i related to the i-th constraint is decreased almost surely (in a statistical sense). The adaptation rule for the weight w_i after each generation is defined as: $w_i = w_i \exp(p_{target} - r_i^{feas})$, where p_{target} is a value that changes at each iteration according to $p_{target} = (1/Kn_P)^{1/\mathscr{D}}$, where $\mathscr{D}$ represents the cardinality of the elements' set that satisfies $i = 1,\dots,n_C : \bar{r}_i^{feas} < 1$ and K is the number of samples. As a rule of thumb, when $r_i^{feas} > p_{target}$ the weight w_i decreases, otherwise it increases. In Fig. 4 we provide a pseudo-code for this variant, where we refer to the weight computation routine as $\mathrm{UPDATEWEIGHT}(\cdot)$. For more detail on the method we refer to [12].

This method is more interesting since the penalty factor applied to the objective function changes during the optimization process depending on the number of feasible solutions that do not violate the constraints, considering the relaxation acting on the equality constraints. With respect to the vanilla method, the penalty factor here is not constant over the parameter space and depends on the exploration path in the parameter space. This decreases the possibility of getting stuck in local minima or flat areas of the fitness.

D. (1+1)-CMA-ES with Covariance Constrained Adaptation

The third method, proposed by Arnold *et al.* [2], is an extension of (1+1)-CMA-ES with active covariance adaptation [16]. As opposed to the other two methods, here we do not have a penalty factor, *i.e.*, the objective function is unchanged, but there is a different exploration strategy that exploits the constraints information to change the covariance and keep the optimization in a feasible region.

A notable difference with the classical CMA-ES is the fact that there is only one sample per generation ($\boldsymbol{\pi}_1$, therefore $K = 1$), that is generated according to the following rule:

$$\boldsymbol{\pi}_1 = \boldsymbol{\pi} + \sigma\mathbf{D}\mathbf{z} \quad (4)$$

where $\mathbf{D}$ is the Cholesky factor of the covariance matrix $\boldsymbol{\Sigma} = \mathbf{D}^T\mathbf{D}$ and $\mathbf{z}$ is a standard normal distributed vector $\mathbf{z} \sim \mathcal{N}(\mathbf{0}, \boldsymbol{I})$. The algorithm stores the information about the successful steps in a *search path* $\mathbf{s} \in \mathbb{R}^{n_P}$. Each time a

CMA-ES with vanilla constraints

```
function CMA-ES
    for each $gen = 1, \dots, n_{GENERATIONS}$ do
        for $k = 1, \dots, K$ do
            $\boldsymbol{\pi}_k \sim \mathcal{N}(\boldsymbol{\pi}, \sigma^2 \boldsymbol{\Sigma})$
        end for
        for $k = 1, \dots, K$ do
            $J_k = J(\boldsymbol{\pi}_k)$
            if CONSTRVIOLATION($\boldsymbol{\pi}_k$) then
                $\hat{J}_k$ = PENALTY($\boldsymbol{\pi}_k, J_k$)
            end if
        end for
        $\boldsymbol{\pi}_{1:K_e}$ = SORT($\boldsymbol{\pi}_{k=1:K}, \hat{J}_{k=1:K}$)
        $\boldsymbol{\pi}^{new} = \sum_{k=1}^{K_e} P_k \boldsymbol{\pi}_k$ with $\sum_{k=1}^{K_e} P_k = 1$
        $\boldsymbol{\Sigma}^{new}$ = UPDCOV($\boldsymbol{\pi}^{new}, P_{k=1:K_e}$)
        $\sigma^{new}$ = UPDSIGMA($\sigma$)
        $\bar{\boldsymbol{\pi}} = \bar{\boldsymbol{\pi}}^{new}$   $\boldsymbol{\Sigma} = \boldsymbol{\Sigma}^{new}$   $\sigma = \sigma^{new}$
    end for
end function
```

CMA-ES with adaptive constraints

```
function CMA-ES
    for each $gen = 1, \dots, n_{GENERATIONS}$ do
        for $k = 1, \dots, K$ do
            $\boldsymbol{\pi}_k \sim \mathcal{N}(\boldsymbol{\pi}, \sigma^2 \boldsymbol{\Sigma})$
        end for
        for $k = 1, \dots, K$ do
            $J_k = J(\boldsymbol{\pi}_k)$
        end for
        $[l, r, \bar{r}]$ = COLLECTVIOLATION($\boldsymbol{\pi}_k, \boldsymbol{\varepsilon}$)
        $w^{new}$ = UPDATEWEIGHT($w, r, \bar{r}$)
        $\hat{J}_k$ = WEIGHTPENALTY($w^{new}, l$)
        $\boldsymbol{\pi}_{1:K_e}$ = SORT($\boldsymbol{\pi}_{k=1:K}, \hat{J}_{k=1:K}$)
        $\boldsymbol{\pi}^{new} = \sum_{k=1}^{K_e} P_k \boldsymbol{\pi}_k$ with $\sum_{k=1}^{K_e} P_k = 1$
        $\boldsymbol{\Sigma}^{new}$ = UPDCOV($\boldsymbol{\pi}^{new}, P_{k=1:K_e}$)
        $\sigma^{new}$ = UPDSIGMA($\sigma$)
        $\bar{\boldsymbol{\pi}} = \bar{\boldsymbol{\pi}}^{new}$   $\boldsymbol{\Sigma} = \boldsymbol{\Sigma}^{new}$   $\sigma = \sigma^{new}$
    end for
end function
```

(1+1)-CMA-ES with Cov. Const. Adapt.

```
function (1+1)-CMA-ES
    $\boldsymbol{\pi}$ = FINDFEASIBLESTARTINGPOINT()
    for each $gen = 1, \dots, n_{GENERATIONS}$ do
        $\boldsymbol{\pi}_1 = \boldsymbol{\pi} + \sigma \mathbf{D}\mathbf{z}$ (Eq.4)
        if CONSTRVIOLATION($\boldsymbol{\pi}_1$) then
            $\mathbf{D}^{new}$ = UPCOVCONSTR(); $\mathbf{D} = \mathbf{D}^{new}$
        else
            $J^{new} = J(\boldsymbol{\pi}_1)$
            if $J^{new} > J$ then
                $\mathbf{D}^{new}$ = UPCOVSUCC()
                $\sigma^{new}$ = UPDSIGMA($\sigma$)
                $\boldsymbol{\pi} = \boldsymbol{\pi}_1$; $\mathbf{D} = \mathbf{D}^{new}$; $\sigma = \sigma^{new}$
            else if $J^{new} > J^{old}$ then
                $\mathbf{D}^{new}$ = UPCOVACTIVE(); $\mathbf{D} = \mathbf{D}^{new}$
            end if
        end if
    end for
end function
```

Fig. 4. Pseudocode for the three variants of constrained CMA-ES: the first is with vanilla penalty (Section III-B), the second is the adaptive penalties method of [12] (Section III-C) and the third is a (1+1)-CMA-ES with covariance constrained adaptation as in [2] (Section III-D).

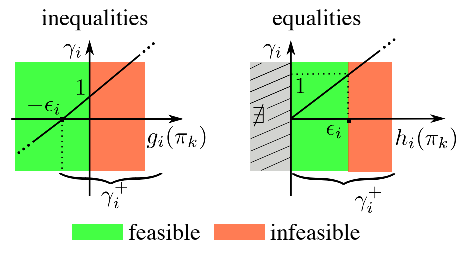

Fig. 5. This illustration shows the relation between ε_i and γ_i for inequality and equality constraints as in Eq. 3. As described in Section III-C, the green and red regions identify the constraint values that are respectively labeled as "feasible" and "infeasible". One may notice that ε_i induces a relaxation for the equality constraint: therefore it could be possible to label as feasible a solution that violates the constraint (how much depends on ε). On the contrary, it is noticeable that γ_i^+ in the inequality constraint also includes a boundary region determined by ε_i where the constraint is satisfied.

candidate outperforms the current best, $\mathbf{s}$ and $\mathbf{D}$ are updated (UPCOVSUCC in Fig. 4):

$$\mathbf{s}^{new} = (1-c)\mathbf{s}\sqrt{c(2-c)}\mathbf{D}\mathbf{z}$$

$$\mathbf{D}^{new} = \sqrt{1-c_{cov}^{+}}\mathbf{D} + \frac{\sqrt{1-c_{cov}^{+}}}{||\mathbf{w}||^2}\left(\sqrt{1+\frac{c_{cov}^{+}||\mathbf{w}||^2}{1-c_{cov}^{+}}}-1\right)\mathbf{s}\mathbf{w}^T$$

where c_{cov}^{+} and c are both factors that control the update rate of $\mathbf{s}$ and $\mathbf{D}$ respectively, while $\mathbf{w} = \mathbf{D}^{-1}\mathbf{s}$. Instead, if the current candidate is feasible but its performance is lower than the predecessors, the Cholesky factor $\mathbf{D}$ is actively updated (UPCOVACTIVE in Fig. 4):

$$\mathbf{D}^{new} = \sqrt{1+c_{cov}^{-}}\mathbf{D} + \frac{\sqrt{1+c_{cov}^{-}}}{||\mathbf{z}||^2}\left(\sqrt{1-\frac{c_{cov}^{-}||\mathbf{z}||^2}{1+c_{cov}^{-}}}-1\right)\mathbf{D}\mathbf{z}\mathbf{z}^T$$

where c_{cov}^{-} is again a constant that determines the update rate. In this case $\mathbf{s}$ is not updated because the current candidate is not better in terms of fitness.

To handle constraints, the key idea is to update the covariance matrix, by reducing the components of $\mathbf{D}\mathbf{z}$ in the direction that is orthogonal to the constraint whenever a constraint is violated, as illustrated in Fig. 6. Each time the j-th constraint is violated, we update the corresponding constraint vector $\mathbf{v_j} \in \mathbb{R}^{n_P}$ and the matrix $\mathbf{D}$ (UPCOVCONSTR in Fig. 4):

$$\mathbf{v}_j^{new} = (1-c_c)\mathbf{v}_j + c_c\mathbf{D}\mathbf{z}$$

$$\mathbf{D}^{new} = \mathbf{D} - \frac{\beta}{\sum_{j=1}^{n_C}\mathbf{1}_{g_j(\boldsymbol{\pi}_1>0)}}\sum_{j=1}^{n_C}\mathbf{1}_{g_j(\boldsymbol{\pi}_1>0)}\frac{\mathbf{v}_j\mathbf{w}^T}{\mathbf{w}^T\mathbf{w}}$$

where c_c and β are constants that tune the update step respectively for $\mathbf{v}_j$ and $\mathbf{D}$, $\mathbf{w}_j = \mathbf{D}^{-1}\mathbf{v}_j$ and $\mathbf{1}_{g_j(\boldsymbol{\pi}_1>0)}$ is equal to one when $g_j(\boldsymbol{\pi}_1) > 0$ and zero otherwise.

In summary, the method searches for the optimal solution by testing one sample at the time and accounting for the constraints in the covariance adaptation to stay away from infeasible regions. The algorithm is designed in such a way that the mean of the search distribution is updated only if the fitness improves and the candidate is a feasible solution; these two elements ensure that the solution of the optimization problem always satisfies the constraints. However, unlike the other methods, this requires a feasible[1] starting candidate to work, otherwise the exploration process quickly gets stuck. Hence, this method cannot be started from scratch or random values, but needs the pre-computation of a feasible starting point. This is not an issue, since we can always find a feasible starting point that satisfies all the constraints, even if it does not enable the robot to achieve the global task goal (a quick solution is to set the robot in a feasible posture and keep this position by setting the posture task priority to 1 and the others to 0).

IV. BENCHMARKING THE ALGORITHMS

In this section we test the algorithms described in Section III to decide which one better suits our problem. We compare their performances on five different benchmarks:

[1]A candidate solution is feasible if it satisfies all the constraints.

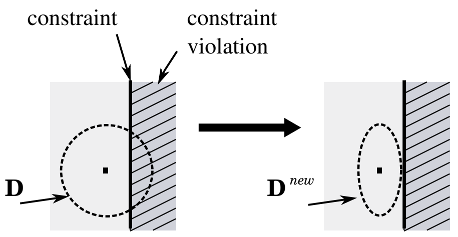

Fig. 6. This illustration shows the effect of the covariance adaptation with constraints, as described in Section III-D. A linear inequality constraint, represented by the vertical thick line, divides the parameter space into a region where the constraint is not violated (light grey) and a region where the constraint is violated (dark grey). The covariance $\mathbf{D}$ of the search distribution is updated in such a way that the successor samples will not fall into the region where the constraint is active: the updated covariance $\mathbf{D}^{new}$ is directed orthogonally with respect to the constraint.

– g07: $n_P = 10, n_{IC} = 8, n_{EC} = 0$
– g09: $n_P = 7, n_{IC} = 4, n_{EC} = 0$
– HB: $n_P = 5, n_{IC} = 6, n_{EC} = 3$
– RB1: $n_P = 15, n_{IC} = 32, n_{EC} = 0$
– RB2: $n_P = 15, n_{IC} = 50, n_{EC} = 0$

The first three are classical benchmarks for constrained optimization [2], that is analytic problems with known optimal solutions; the last two are new benchmarks that we designed *ad hoc* to evaluate the performance of the algorithms on robotic problems with growing complexity. RB1 is a problem inspired by our previous work [1] where a KUKA LWR (7DOF) has to reach a goal position with its end-effector behind an obstacle, while satisfying constraints of joint position limits, joint torque limits and obstacle avoidance. RB2 has a similar setting with the addition of a second obstacle to avoid and another set of constraints coming from joint velocity limits. To compare the performance of the algorithms on these benchmarks, we define the following metrics:

- m_1: *distance from the optimal solution*, defined as $m_1 = \|\boldsymbol{\pi}^\circ - \boldsymbol{\pi}^*\|$, where $\boldsymbol{\pi}^\circ$ is the optimal solution (known) and $\boldsymbol{\pi}^*$ the best solution found by the constrained optimization algorithm;
- m_2: *constraint violations*, defined as $m_2 = \sum_{i=1}^{n_C} |\hat{e}(i, \boldsymbol{\pi}^*)|$, where $\hat{e}(i, \boldsymbol{\pi}) = \mathbf{1}_{g_i(\boldsymbol{\pi})>0}\, g_i(\boldsymbol{\pi})$ for the inequality constraints and $\hat{e}(i, \boldsymbol{\pi}) = \mathbf{1}_{h_i(\boldsymbol{\pi})\neq 0}\, h_i(\boldsymbol{\pi})$ for the equality constraints — basically it sums all the constraints that are violated;
- m_3: *number of steps to converge*, or *settling time*, defined as $m_3 = n_{sc}(\delta)$, the number of steps after which the fitness function reaches a steady state condition, *i.e.*, its value is bounded between $\pm\delta\%$ of the steady state value — here, we set $\delta = 2.5$;
- m_4: *best fitness*, defined as $m_4 = J(\boldsymbol{\pi}^*)$, *i.e.*, the fitness of the best solution found by the constrained optimization algorithm.

To provide a baseline, we use the (deterministic) constrained optimization function *fmincon* in Matlab, using the SQP method. This is a suitable choice because it does not require the gradient of the objective function for non-linear constrained optimization problem with nonlinear constraints.

Since (1+1)-CMA-ES with covariance constrained adaptation (Section III-D) needs a feasible candidate solution as a starting point, in order to make a fair comparison all the algorithms start from the same initial position. We perform 40 repetitions of the optimization process per each test problem for each algorithm with an exploration rate of 0.1 and a 5000 samples to assure the convergence of the methods.

Fig. 7 shows the results of the numerical experiments with the five benchmarks. The top row reports on the results for g07, g09 and HB with metrics m_1, m_2, m_3, while the bottom row reports on the results for the robotics benchmarks RB1 and RB2, with metrics m_2, m_3, m_4 (m_1 cannot be used in this case because the optimal solution $\boldsymbol{\pi}^\circ$ is not known). We also compared the four algorithms in terms of computational time, and did not find significant differences (for example, the optimal solution for RB2 is found on average in $\approxeq$1.7e+04 *s* for the CMA-ES variants and 1.9e+04 *s* for *fmincon* on a i5 laptop with Matlab).

(1+1)-CMA-ES with covariance constrained adaptation offers the best trade-off between performance and constraints' satisfaction both on the analytic and the robotic benchmarks. It always ensures full satisfaction of the constraints while the other methods sometimes fail. Its settling time is comparable to the other stochastic algorithms, while *fmincon* converges faster. *fmincon* could seem more appealing, but on the robotic benchmarks its best fitness is lower and actually quite close to the fitness of the starting point (meaning that the algorithm does not really "explore"). Therefore *fmincon* does not seem a suitable candidate for solving robotic problems with a lot of constraints.

The different performances of the algorithms in the analytic and robotic benchmarks confirm the benefit gained by designing two new robotics benchmarks RB1,RB2. Overall, considering the zero constraint violations and the capability of finding a good solution, we choose to use (1+1)-CMA-ES with covariance constrained adaptation for our experiments with the iCub robot.

V. Robotic experiments

In this section, we apply (1+1)-CMA-ES with covariance constrained adaptation to our multi-task control framework (Section II). We use it to optimize the task priorities and to obtain a solution that never violates the constraints. In the following, we report on the experiments performed to optimize the whole-body movements of the iCub humanoid robot.

We designed two experiments using the 17 DOF of the upper-body of the robot (arms and torso). In the experimental scenario, a rectangular obstacle similar to a wall, that is as large as the robot's chest and 2 *cm* thick, is placed about 20 *cm* in front of the robot.

The first experiment is aimed at reaching a goal Cartesian position behind the wall with one hand. There are three elementary tasks. The first is about reaching the desired Cartesian position $\mathbf{p}_r^* = [0.35, -0.15, 0.7]$ (m) with the right hand frame of the robot. The second task is reaching a desired

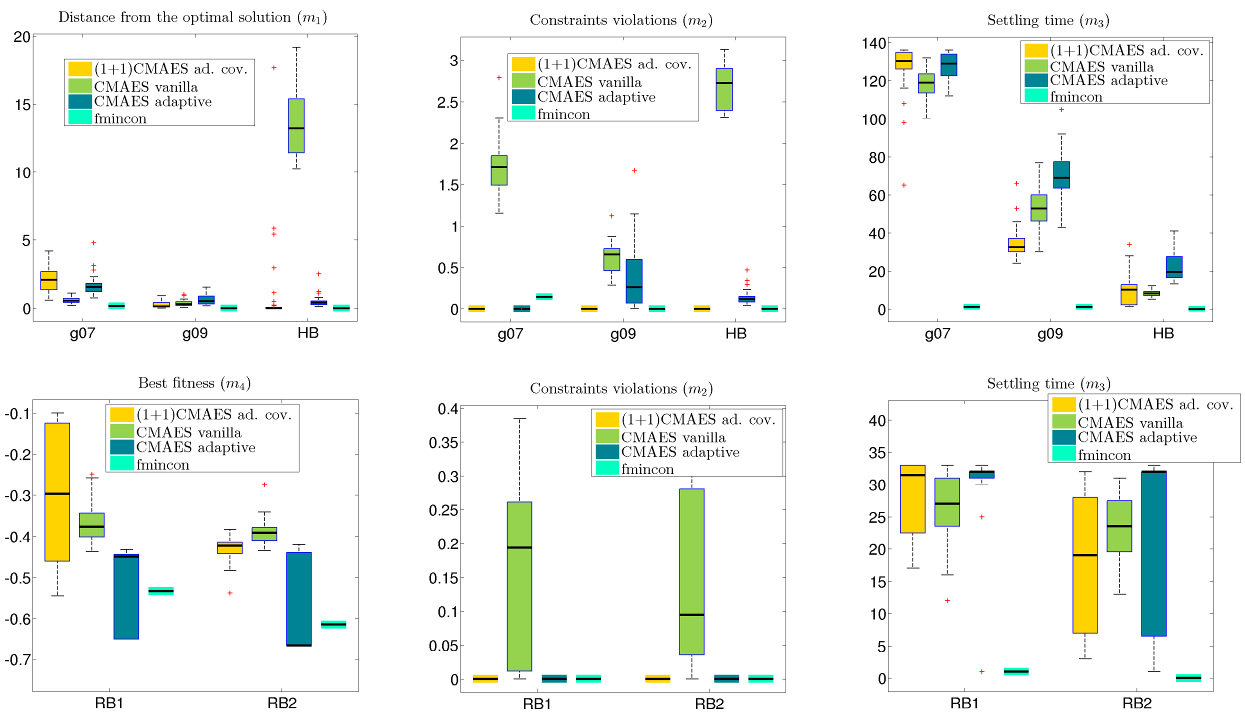

Fig. 7. Performance comparison of the three constrained CMA-ES algorithms and the baseline *fmincon* algorithm from Matlab using the SQD method. The top row reports on the results on three standard analytical constrained optimization benchmarks (g07, g09, HB - see [2]). The bottom row reports on the results on two robotics benchmarks (RB1, RB2) that we designed *ad hoc* to evaluate the performance of the algorithms on robotics problems.

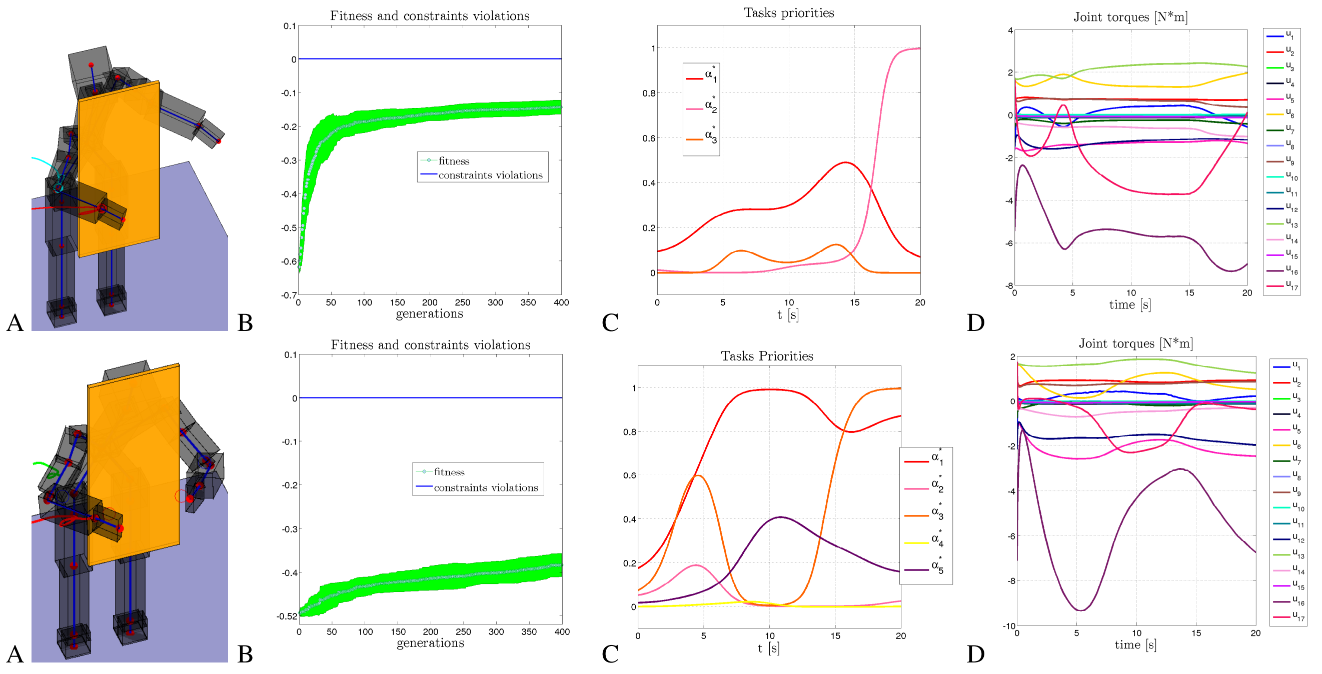

Fig. 8. Two experiments with the iCub, about reaching a goal behind the wall with one or two hands. A) The robot's movement visualized by the mex model. B) The median constraint violation and fitness optimized by (1+1)-CMA-ES with covariance constrained adaptation (over 25 experiments) the constraints are never violated C-D. The task priorities and joint torques of the best solution. The experiments are also shown in the attached video.

Cartesian position $\mathbf{p}^*_{elbr} = [0.24, -0.23, 0.7]$ (m) with the elbow frame. The third task is keeping the initial joint configuration $\mathbf{q}^* = [0, 45, 0, 0, -20, 30, 0, 0, 45, 0, 0, 0, 30, 0, 0, 0, 0]$ (deg). In sum, the goal is hidden behind the wall, and to reach it with the hand the robot must bend its elbow around the wall corner; the third task should prevent the robot from moving the right arm and the torso. The task priorities are approximated by RBFs with $n_r = 5$, therefore $n_P = 5 \times 3 = 15$. There are $n_C = n_{IC} = 73$ inequality constraints: joint position limits, joint torque limits and distance constraints to avoid collisions between the robot and the obstacle. Precisely, a minimal distance of 3 *cm* is required between the obstacle and a set of pre-defined collision check points (located at the origin of the frames of right shoulder, elbow, wrist, hand and head). For this experiment we use the following fitness function:

$$\phi = -\frac{1}{2}\left[\frac{\sum_i^T \|\mathbf{p}_{r,i} - \mathbf{p}_r^*\|}{\varepsilon_{max}} + \frac{\sum_i^T \mathbf{u}_i^2}{u_{max}}\right] \qquad (5)$$

where $\phi \in [-1, 0]$, T is the number of control steps (the task duration is 20 *s*, and we control at 1 *ms*), $\mathbf{p}_{r,i}$ is the right hand frame position at time i, $\mathbf{p}_r^*$ the goal position for the hand frame and $\varepsilon_{max} = 120$ and $u_{max} = 3.5 * 10^5$ are two scaling factors. The first term of ϕ penalizes the cumulative distance from the goal, while the second term penalizes the global control effort.

The second experiment complicates the first by adding 2 more tasks. The aim is to reach a Cartesian goal position with both robot hands. Two Cartesian goal tasks for each hand and elbow are set symmetrically with respect to iCub's sagittal plane. A fifth posture task is set as to keep the torso as straight as possible during the movement.

- Task 1 : $\mathbf{p}_r^* = [0.35, -0.15, 0.68]$ (m)
- Task 2 : $\mathbf{p}_{elbr}^* = [0.21, -0.25, 0.68]$ (m)
- Task 3 : $\mathbf{p}_l^* = [0.3, 0.0248, 0.68]$ (m)
- Task 4 : $\mathbf{p}_{elbl}^* = [0.21, 0.1138, 0.68]$ (m)
- Task 5 : $\mathbf{q}^* = [0, 45, 0, 0, -20, 30, 0, 0, 45, 0, 0, 0, 30, 0, 0, 0, 0]$ (deg)

The task priorities are approximated by RBFs with $n_r = 5$, therefore $n_P = 5 \times 5 = 25$. The optimization is carried out under the same constraints as in the first experiment with the addition of the left arm collision checks. This means we have $n_C = n_{IC} = 77$ inequality constraints. The fitness is:

$$\phi = -\frac{1}{2}\left(\frac{\sum_i^T \|\mathbf{p}_{r,i} - \mathbf{p}_r^*\|}{\varepsilon_{max}} + \frac{\sum_i^T \|\mathbf{p}_{l,i} - \mathbf{p}_l^*\|}{\varepsilon_{max}} + \frac{\sum_i^T \mathbf{u}_i^2}{u_{max}}\right) \qquad (6)$$

where $\mathbf{p}_{l,i}$ is the left hand frame position at time i, $\mathbf{p}_l^*$ the goal position for the left hand frame.

In all the experiments, we seek the best solutions that do not violate any of the constraints. We employ (1+1)-CMA-ES as described in Section III-D with the exploration rate set to 0.1 (this is the only parameter to tune and this is the default value!).

Fig. 8 shows the median fitness and constraint violation obtained by 25 experiments. The fitness grows nicely ($\phi = 0$ would be the optimum). Most importantly, the **constraints are never violated**, which is exactly what we wanted to obtain. We also show the task priorities and the joint torques from one of the best solutions; they are both smooth, and it is clear that optimizing the task priorities manually would be very difficult if these solutions were to be achieved. The video attachment shows the robot movements in the two experiments and the activation of the tasks priorities evolving in time.

VI. Conclusion and Future Work

In this paper we proposed to optimize the task priorities of multi-task controllers by a stochastic constrained optimization algorithm that ensures that the constraints are never violated. We benchmarked four constrained optimization algorithms in robotics applications and found that (1+1)-CMA-ES with covariance constrained adaptation meets our requirements in terms of fitness of the solution and constraint satisfaction. Our framework can be used to generate optimized whole-body movements that always comply with safety requirements, as shown in two bimanual experiments with the iCub. Our current limit is the computation time, therefore the method is suited at this time only for offline synthesis of whole-body behaviors of humanoid robots. Ongoing work is aimed at applying the method for safe trajectory optimization (complementary to task priority optimization) and speeding up the computation.

References

[1] V. Modugno, G. Neumann, E. Rueckert, G. Oriolo, J. Peters, and S. Ivaldi, "Learning soft task priorities for control of redundant robots," in *ICRA*, 2016.

[2] D. V. Arnold and N. Hansen, "A (1+1)-CMA-ES for constrained optimisation," in *GECCO*, 2012, pp. 297–304.

[3] L. Saab, O. Ramos, F. Keith, and N. Mansard et al, "Dynamic whole-body motion generation under rigid contacts and other unilateral constraints," *IEEE Trans. on Robotics*, vol. 29, pp. 346–362, 2013.

[4] A. Del Prete, F. Nori, G. Metta, and L. Natale, "Prioritized motion-force control of constrained fully-actuated robots: Task space inverse dynamics," *Robotics and Auton. Systems*, vol. 63, pp. 150–157, 2015.

[5] J. Salini, V. Padois, and P. Bidaud, "Synthesis of complex humanoid whole-body behavior: A focus on sequencing and tasks transitions," in *ICRA*, 2011, pp. 1283–1290.

[6] M. Liu, Y. Tan, and V. Padois, "Generalized hierarchical control," *Autonomous Robots*, vol. 40, pp. 17–31, 2016.

[7] N. Dehio, R. F. Reinhart, and J. J. Steil, "Multiple task optimization with a mixture of controllers for motion generation," in *IROS*, 2015.

[8] S. Ha and C. Liu, "Evolutionary optimization for parameterized whole-body dynamic motor skills," in *ICRA*, 2016.

[9] R. Lober, V. Padois, and O. Sigaud, "Variance modulated task prioritization in whole-body control," in *IROS*, 2015.

[10] N. Hansen and A. Ostermeier, "Completely derandomized self-adaptation in evolution strategies." *Evolutionary Computation*, vol. 9, pp. 159–195, Jan 2001.

[11] F. Berkenkamp, A. P. Schoellig, and A. Krause, "Safe controller optimization for quadrotors with Gaussian processes," in *ICRA*, 2016.

[12] G. Collange, N. Delattre, N. Hansen, I. Quinquis, and M. Schoenauer, "Multidisciplinary optimization in the design of future space launchers," in *Multidisciplinary Design Optimization in Computational Mechanics*. Wiley-Blackwell, 2013, pp. 459–468.

[13] J. Peters, M. Mistry, F. Udwadia, J. Nakanishi, and S. Schaal, "A unifying framework for robot control with redundant DOFs," *Autonomous Robots*, vol. 24, pp. 1–12, Jan 2008.

[14] S. Chiaverini, B. Siciliano, and O. Egeland, "Redundancy resolution for the human-arm-like manipulator," *Robotics and Autonomous Systems*, vol. 8(3), pp. 239–250, Jan 1991.

[15] Y. Nakamura and H. Hanafusa, "Inverse kinematic solutions with singularity robustness for robot manipulator control," *J. Dyn. Sys., Meas., Control*, vol. 108 (3), pp. 163–171, 1986.

[16] C. Igel, T. Suttorp, and N. Hansen, "A computational efficient covariance matrix update and a (1+1)-CMA for evolution strategies," in *GECCO*, 2006.

Chapter 5

Probabilistic Prioritization of Movement Primitives (TUDA)

Probabilistic Prioritization of Movement Primitives

Alexandros Paraschos[1], Jan Peters[1,2] and Gerhard Neumann[1]

***Abstract*— Movement prioritization is a common approach to combine controllers of different tasks for redundant robots. Each task is assigned a priority, where either strict or "soft" priorities can be used. While movement prioritization is an important concept in the control of whole body movements, it has been less considered in learning-based approaches, where prioritization allows us to learn different tasks for different end-effectors, and subsequently reproduce an arbitrary, unseen combination of these tasks. This paper combines Bayesian task prioritization, a "soft" prioritization technique, with probabilistic movement primitives to prioritize full motion sequences. Probabilistic movement primitives can encode distributions of movements over full motion sequences and provide control laws to exactly follow these distributions. The probabilistic formulation allows for a natural application of Bayesian task prioritization. We demonstrate how the "soft" priorities can be obtained from imitation learning and that our prioritized learning architecture can reproduce unseen task-combinations. Moreover, we require less data to learn a combination of tasks than the traditional approach that directly models each task in joint space. We evaluate our approach on reaching movements under constraints with a redundant bi-manual planar robot and the humanoid robot iCub.**

I. Introduction

Complex robots with redundant degrees of freedom have increased manipulation capabilities and, can in principle perform multiple tasks at the same time. For example, possible task combinations are reaching an object with a humanoid robot while balancing or reaching an object with a robotic arm while the "elbow" avoids an obstacle.

Performing multiple tasks simultaneously is not trivial, as it often requires to simultaneously control the same joints with different control laws, that leads to conflicting control signals. Many control schemes that can combine these signals were developed. We focus on approaches that resolve the control combination problem by prioritizing the tasks. Task prioritization can be either strict, where a lower priority task is not allowed to interfere with higher priority tasks, or "soft", where the aforementioned assumption can be violated. Movement prioritization is an established concept for controlling whole body movements, however, prioritized task combination is also a powerful concept for learning-based approaches, where such concepts have not yet been explored so far. For example, prioritization allows us to learn different tasks for different end-effectors and subsequently reproduce an arbitrary, unseen combination of these tasks.

*The research leading to these results has received funding from the European Community's Seventh Framework Programme (FP7/2007–2013) under grant agreements #600716 (CoDyCo) and #270327 (CompLACS)

[1]Intelligent Autonomous Systems, TU Darmstadt, 64289 Darmstadt, Germany {paraschos,neumann}@ias.tu-darmstadt.de

[2] Robot Learning Group, Max Planck Institute for Intelligent Systems, Germany mail@jan-peters.net

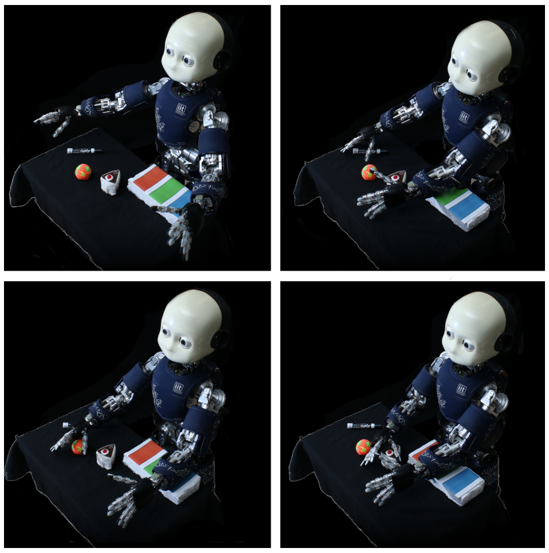

Fig. 1. The iCub robot performing a bi-manual reaching task. With the left end-effecotr, the robot initiates a supportive contact with the environment, while it performs a reaching task with the right end-effector. We illustrated our setup if the first picture. The robot stands on the floor and had the choice of three supporting contact locations, shown in blue, green, and red. With the right end-effector the robot can reach for grasping three different objects, a pen, a ball, and a piece of cake. In the remaining pictures we present our results for learning and generalizing to new task combinations of reaching and contact support locations.

In this paper, we propose a new imitation learning architecture that learns a prioritized skill representation. We combine Bayesian task prioritization [1], a "soft" prioritization method, with Probabilistic Movement Primitives (ProMPs) [2], [3] to prioritize motion sequences that are learned from demonstrations. Bayesian task prioritization has been introduced in [1] but gained little attention in that paper and follow up work. We provide a more general derivation for torque control and show that existing prioritization techniques are a special case of the Bayesian approach.

Our prioritization is data-driven, i.e. it employs demonstrations to the robot to extract the relative prioritization from imitation data. The demonstrations can be acquired by several imitation learning techniques, including kinesthetic teach-in and tele-operation. We use multiple demonstrations for every task to accurately extract the variance of its movement, where different tasks can be learned for different end-effectors. In contrast to other approaches, we present a closed form solution for setting each task's "soft" priority from the variance of the task in its operational space. Furthermore, we compute the output control, still in closed form. We represent the variance of a task at each state using ProMPs. ProMPs encode a trajectory distribution and, thus, represent the time-varying variance of each task. The primitives can be trained using imitation learning, and, generate probabilistic controllers that follow exactly the encoded task distribution. The variances of the probabilistic controllers can be used naturally for Bayesian task prioritization.

We can learn multiple primitives for a single end-effector, where each primitives solves a specific task with the corresponding end-effector. The primitives of different end-effectors can now be seamlessly combined in order to achieve a new, unseen combination of tasks of the end-effectors. Another advantage of ProMPs is that we can adapt the distribution by conditioning on reaching different via-points. Using the prioritization of ProMPs, conditioning can now be done also for task space variables instead of simply in joint space. We demonstrate that our data-driven prioritization approach can be used for conditioning in task-space as well as the improved multi-task learning capabilities or our approach in simulation and on a reaching and stabilizing task with the iCub.

II. Related work

A common resolution for combining different control signals is to prioritize the tasks, under the assumption that this prioritization is not allowed to be violated. We refer to such schemes as a strict prioritization schemes. In these schemes, a higher priority task does not get disturbed by the control signals of the lower priority ones [4], [5], [6], [7], [8], [9], [10], [11], [12]. A lower priority task is always projected in the null-space of the high priority task. Although these approaches provide guarantees on the system performance, they are often over-constraining and therefore limit its usefulness in real-word applications. Moreover, strict prioritization approaches might get numerically instable when the robot enters a singular kinematic configuration. Proposed solutions to the numerical stability problem exist [13], [14], but also have a side-effect: they relax to some extent the assumption that a low priority task does not interfere with a higher priority task.

For some tasks, such a prioritization scheme is natural, for example, a humanoid robot should not tip over and, therefore, the balancing controller should always have the highest priority. However, defining a strict priority can be problematic in general. For example, for reaching an object with one hand of a humanoid robot, while simultaneously reaching for a different object with the other hand, it is not clear these tasks can be prioritized. Both tasks could have the same importance, i.e. priority, or, the importance of each tasks could vary in time and depending on, e.g., the desired execution accuracy at that time point. For such scenarios, the relative importance between the tasks is easier to set and requires less hand-tuning. These problems are partially addressed in [15], [16], [17], where a "soft" prioritization scheme was introduced. In our approach, we step further and propose to learn the relative priorities from data and, therefore, minimize the amount of parameters that require expert knowledge to be tuned.

"Soft" prioritization approaches do not assume a priori a hierarchy of tasks but they use the relative priorities between the tasks. In this scheme, every task contributes to the control signal. The degree of contribution depends on its relative priority. "Soft" prioritization approaches demonstrate promising results where strict approaches fail [15], [18], [19] to successfully perform multiple tasks due to the relaxation of the initial problem. Intuitively, "soft" prioritization schemes could be thought as violating the hierarchy of priorities. They are often formulated as multi-objective optimization problems [15], [18], [19]. Each task is formulated as a quadratic cost function and uses the relative priority as weight. The result of the optimization yields the controls that minimize the total cost and, therefore, allows lower priority tasks to perturb higher priority ones as long as the total cost is decreased.

Both strict and "soft" prioritization approaches often assume a static prioritization or weighting scheme, where the importance of each task remains constant during the execution of the movement [6], [17]. However, modulating the importance of the tasks during the movement can be beneficial. First, tasks that are no longer desired to be executed can be faded-out and new tasks can be smoothly introduced, without torque jumps. Salini et al. [15] proposed to dynamically adjust the priorities for achieving movement sequencing and tasks transitions. Second, and more importantly, the modulation of the priorities can be related to the desired accuracy of the task. During the time-steps with low task-priority, the robot can focus on executing other tasks. Therefore, setting the relative priorities can be a simpler problem then specifying the strict task hierarchy, as the expert has to specify only the time points that require higher accuracy. Lober et al. [19] demonstrated that this approach increases the flexibility of the system and decreases "lock-ups" where a more important movement prohibits the execution of less important tasks, while it requires less expert knowledge. Modugno et al. [20] proposed the use of an optimization algorithm to find suitable "soft" priorities that further decreases expert knowledge.

Movement primitives are a well established concept for imitation learning and generalization of movements in robotics [21], [22], [23], [2], however, no primitive representation has so far taken leverage from introducing task priorities. In this paper, we introduce for the first time task-priorities for movement primitives. We use the Probabilistic Movement Primitive approach as it can be naturally combined with Bayesian task prioritization in a single probabilistic framework. However, other stochastic movement representations could also be used instead [22], [24].

III. Probabilistic Prioritization of Stochastic Controllers

In this section, we develop a generic probabilistic framework for simultaneously combining multiple tasks. We assume that each tasks has a different degree of accuracy and that the accuracy changes over time. We associate the task accuracy with its importance for the task combination.

First, we show how the time-varying task accuracy can be encoded in an efficient representation and, importantly, how this accuracy, which is learned from imitation data, can be translated to the task priority. Second, we develop our stochastic combination approach using the task accuracy as relative priorities. Third, we show that both strict and "soft" prioritization approaches are special cases of our prioritization approach where some uncertainty parameters are set to zero.

To better illustrate our approach, we begin our description by prioritizing two controllers; an operational-space controller which has the highest priority and a low priority joint-space controller. Subsequently, we extend our approach to multiple operational-space controllers in Sec. III-C. We use operation-space prioritization as an illustration of our approach, but in Sec. IV we show that our stochastic prioritizing scheme can be generalized to a wider class of controllers.

A. Encoding Task Accuracy from Demonstrations

Representing the desired task accuracy throughout the duration of the task is critical for our approach. A measure for the task accuracy is the task variance that is be obtained over multiple executions of the task. Stochastic movement primitive representations can not only represent the task variance but also enable training from demonstration data. To this end, we use the Probabilistic Movement Primitives (ProMPs) approach [2], [3] as our representation.

ProMPs represent a single trajectory as a weighed linear combination of Gaussian basis functions $\boldsymbol{\Phi}_t$ and the respective weights $\boldsymbol{w}$, i.e.,

$$\boldsymbol{y}_t = \boldsymbol{\Phi}_t \boldsymbol{w}, \tag{1}$$

where $\boldsymbol{y}_t = [\boldsymbol{x}, \dot{\boldsymbol{x}}]^T$ represents the state of the task, i.e., positions and velocities, at time t. The task state $\boldsymbol{y}_t$ is a vector that contains the variables that define the state of the tasks, e.g., the joint or end-effector positions and velocities. Each task demonstration is used to estimate the weights $\boldsymbol{w}$ for that execution using a maximum likelihood approach [2]. From the set of estimated weights, ProMPs estimate a distribution over the weights, i.e.,

$$p(\boldsymbol{w}) = \mathcal{N}\left(\boldsymbol{w} | \boldsymbol{\mu}_{\boldsymbol{w}}, \boldsymbol{\Sigma}_{\boldsymbol{w}}\right), \tag{2}$$

which is assumed to be approximated well by a Gaussian, or a mixture of Gaussian [25], [26]. Thus, ProMPs offer a compact representation of the trajectory distribution in task space, that is, the mean movement in task space, the correlation between the task's variables, and their variance. With ProMPs, we can evaluate the distribution of the state $p(\boldsymbol{y}_t)$ at every time-step

$$p(\boldsymbol{y}_t) = \int p(\boldsymbol{y}_t|\boldsymbol{w}) p(\boldsymbol{w}) \mathrm{d}\boldsymbol{w} = \mathcal{N}\left(\boldsymbol{y}_t | \boldsymbol{\mu}_{\boldsymbol{y}_t}, \boldsymbol{\Sigma}_{\boldsymbol{y}}\right) \tag{3}$$

in closed form. ProMPs also provide a stochastic linear controller, which is also derived in closed form. The controller can follow the encoded task distribution exactly, i.e., it matches mean and variance of the distribution. In [2], [3], ProMPs are used to control the joints of the robot and, therefore, the controller outputs are joint torques. In our approach, we generalize ProMPs to model and control task variables, e.g. the robot end-effector. To do so, we adjust the ProMP controller's output to the acceleration of task space variables. The stochastic controller is, therefore, given by

$$p(\ddot{\boldsymbol{x}}|\boldsymbol{y}_t) = \mathcal{N}\left(\ddot{\boldsymbol{x}} | \boldsymbol{K}_t \boldsymbol{y}_t + \boldsymbol{k}_t, \boldsymbol{\Sigma}_{\ddot{\boldsymbol{x}}}\right). \tag{4}$$

The mean of the controller is given by a linear feedback control law. The controller additionally contains the covariance of the task in the acceleration space. The later plays an important part in our approach as it specifies the required accuracy of the control, see Sec. III-B. In summary, ProMPs are capable of representing and learning the task covariance $\boldsymbol{\Sigma}_{\boldsymbol{y}}$, and transforming it to the acceleration covariance $\boldsymbol{\Sigma}_{\ddot{\boldsymbol{x}}}$.

B. Probabilistic Combination of Tasks

We begin our derivation given two tasks, a joint-space task and an operational-space task. For each task, a stochastic controller is obtained from the corresponding ProMP that has been trained from demonstrations. Each controller is normally distributed, i.e., the probability of each controller is given by

$$p_1(\ddot{\boldsymbol{q}}) \sim \mathcal{N}\left(\ddot{\boldsymbol{q}} | \boldsymbol{\mu}_{\ddot{\boldsymbol{q}}}, \boldsymbol{\Sigma}_{\ddot{\boldsymbol{q}}}\right), \quad p_2(\ddot{\boldsymbol{x}}) \sim \mathcal{N}\left(\ddot{\boldsymbol{x}} | \boldsymbol{\mu}_{\ddot{\boldsymbol{x}}}, \boldsymbol{\Sigma}_{\ddot{\boldsymbol{x}}}\right). \tag{5}$$

The vector $\ddot{\boldsymbol{q}}$ denotes the joint acceleration, for all of the joints of the robot and the vector $\ddot{\boldsymbol{x}}$ the operational-space acceleration. Equation (5) is true for every time-step, however, we dropped the time-index for simplicity.

The operational-space controller and the joint-space controller can not be used simultaneously without accounting for the kinematics of the system. The system kinematics introduce a constraint between the operational and the joint space acceleration. The constraint is commonly defined in the velocity space by $\dot{\boldsymbol{x}} = \boldsymbol{J}\dot{\boldsymbol{q}}$, where $\boldsymbol{J}$ denotes the Jacobian from a base-frame to the operational-space. Equivalently, by differentiation over time, we obtain the acceleration-space formulation $\ddot{\boldsymbol{x}} = \boldsymbol{J}\ddot{\boldsymbol{q}} + \dot{\boldsymbol{J}}\dot{\boldsymbol{q}}$ of the constraint. The term $\dot{\boldsymbol{J}}$ denotes the time derivative of the Jacobian[1]. Given the constraint in the acceleration-space, the operational-space controller depends on the current joint-acceleration $\ddot{\boldsymbol{q}}$. The probability of the operational-space acceleration $\ddot{\boldsymbol{x}}$ given the joint acceleration $\ddot{\boldsymbol{q}}$ is given by the conditional

$$p_{2|\ddot{\boldsymbol{q}}}(\ddot{\boldsymbol{x}}|\ddot{\boldsymbol{q}}) \sim \mathcal{N}\left(\ddot{\boldsymbol{x}} \middle| \boldsymbol{J}\ddot{\boldsymbol{q}} + \dot{\boldsymbol{J}}\dot{\boldsymbol{q}}, \boldsymbol{\Sigma}_{\ddot{\boldsymbol{x}}}\right), \tag{6}$$

where the mean of the conditional distribution is given by the constraint and the variance is given by the desired task accuracy. We can now use the joint space ProMP as prior distribution and the desired task-space mapping $p_{2|\ddot{\boldsymbol{q}}}(\ddot{\boldsymbol{x}} = \boldsymbol{\mu}_{\ddot{\boldsymbol{x}}}|\ddot{\boldsymbol{q}})$ as likelihood to obtain the posterior distribution for the joint space controller using Bayes theorem, i.e.,

[1]The time derivative of the Jacobian $\boldsymbol{J}$ can be obtained by applying the chain-rule, i.e.,

$$\dot{\boldsymbol{J}} = \frac{\partial \boldsymbol{J}}{\partial \boldsymbol{q}} \frac{\partial \boldsymbol{q}}{\partial t}$$

$$p_{1|\ddot{x}}(\ddot{\boldsymbol{q}}|\ddot{\boldsymbol{x}} = \boldsymbol{\mu}_{\ddot{x}}) = \frac{p_{2|\ddot{q}}(\ddot{\boldsymbol{x}} = \boldsymbol{\mu}_{\ddot{x}}|\ddot{\boldsymbol{q}})p_1(\ddot{\boldsymbol{q}})}{p_2(\ddot{\boldsymbol{x}})} = \mathcal{N}\left(\ddot{\boldsymbol{q}}|\boldsymbol{\mu}, \boldsymbol{\Sigma}\right), \tag{7}$$

where, since both the prior distribution $p(\ddot{\boldsymbol{q}})$ and the conditional $p(\ddot{\boldsymbol{x}}|\ddot{\boldsymbol{q}})$ are Gaussian distributions, the posterior is also a Gaussian distribution. The control law for the joint accelerations $\ddot{\boldsymbol{q}}$ is then obtained by computing the marginal distribution

$$p_{1|2}(\ddot{\boldsymbol{q}}) = \int p_{1|\ddot{x}}(\ddot{\boldsymbol{q}}|\ddot{\boldsymbol{x}})p_2(\ddot{\boldsymbol{x}})\mathrm{d}\ddot{\boldsymbol{x}} = \mathcal{N}\left(\ddot{\boldsymbol{q}}|\boldsymbol{\mu}'_{\ddot{q}}, \boldsymbol{\Sigma}'_{\ddot{q}}\right), \tag{8}$$

that is a Gaussian as well. The mean $\boldsymbol{\mu}'_{\ddot{q}}$ and the covariance $\boldsymbol{\Sigma}'_{\ddot{q}}$ are computed analytically as

$$\boldsymbol{\mu}'_{\ddot{q}} = \boldsymbol{J}^{\dagger}\left(\boldsymbol{\mu}_{\ddot{x}} - \dot{\boldsymbol{J}}\dot{\boldsymbol{q}}\right) + \left(\boldsymbol{I} - \boldsymbol{J}^{\dagger}\boldsymbol{J}\right)\boldsymbol{\mu}_{\ddot{q}} \tag{9}$$

$$\boldsymbol{\Sigma}'_{\ddot{q}} = \left(\boldsymbol{I} - \boldsymbol{J}^{\dagger}\boldsymbol{J}\right)\boldsymbol{\Sigma}_{\ddot{q}} + \boldsymbol{J}^{\dagger}\boldsymbol{\Sigma}_{\ddot{x}}\boldsymbol{J}^{\dagger,T} \tag{10}$$

where the $\boldsymbol{J}^{\dagger}$ denotes the generalized inverse of the Jacobian

$$\boldsymbol{J}^{\dagger} = \boldsymbol{\Sigma}_{\ddot{q}}\boldsymbol{J}^T\left(\boldsymbol{\Sigma}_{\ddot{x}} + \boldsymbol{J}\boldsymbol{\Sigma}_{\ddot{q}}\boldsymbol{J}^T\right)^{-1}. \tag{11}$$

In our approach, the joint space acceleration $\ddot{\boldsymbol{q}}$ and the task-space acceleration $\ddot{\boldsymbol{x}}$, are obtained from the stochastic feedback controller of the ProMPs. However, our approach can be modify to incorporate other stochastic feedback controllers as we evaluate in Sec. V-B. The variance of the operational-space controller $\boldsymbol{\Sigma}_{\ddot{x}}$ is used as regularization matrix and the variance of the joint-space controller $\boldsymbol{\Sigma}_{\ddot{q}}$ as weighting. The generalized inverse $\boldsymbol{J}^{\dagger}$ is not a pseudo-inverse as $\boldsymbol{J}\boldsymbol{J}^{\dagger} \neq \boldsymbol{I}$, due to the regularization by the operational-space covariance $\boldsymbol{\Sigma}_{\ddot{x}}$. Therefore, the matrix $\left(\boldsymbol{I} - \boldsymbol{J}^{\dagger}\boldsymbol{J}\right)$ is not a proper null-space projection of the Jacobian $\boldsymbol{J}$.

C. Extension to multiple tasks

Multiple operational-space controllers can be naturally integrated in our approach where each task $i \in 1 \cdots N$ can operate in a difference space. In principle, it is sufficient to compute the posterior distribution over the joint acceleration $\ddot{\boldsymbol{q}}$, given the accelerations of all task controllers $\{\ddot{\boldsymbol{x}}_i\}_{1\cdots N}$, i.e., $p(\ddot{\boldsymbol{q}}|\{\ddot{\boldsymbol{x}}_i\}_{1\cdots N})$, which can be computed recursively, or in a single step [1], where the single step solution require sparse-matrix inversion techniques for efficiency.

We proceed with the recursive computation. For the recursive computation, we begin with our prior distribution over the joint accelerations $p_1(\ddot{\boldsymbol{q}})$. We condition it with the operational-space acceleration distribution $p_N(\ddot{\boldsymbol{x}}_N)$ of the highest priority task. The resulting posterior distribution $p_{1|N}(\ddot{\boldsymbol{q}}|\ddot{\boldsymbol{x}}_N)$ is then used as a new prior distribution and is conditioned with $p_{N-1}(\ddot{\boldsymbol{x}}_{N-1})$. We continue conditioning until we reach the task $i = 1$. During the computation of the new prior distribution at every step, we can perform a numerical stability analysis of the $(\boldsymbol{\Sigma}_{\ddot{x}}+\boldsymbol{J}\boldsymbol{\Sigma}_{\ddot{q}}\boldsymbol{J}^T)$ matrix inversion, e.g. by computing the condition number of the matrix. If the inversion becomes numerically unstable, then the task i_o added at this step is incompatible to the higher priority tasks $N \cdots i_o - 1$. Our recursive approach has similarities with the strict hierarchical prioritization approaches [5], [4], where they recursively project every lower-priority task in the null-space of the higher priority task. The major difference in our approach is the use of the regularized generalized inverse, as presented in Sec. III-B, We use the tasks accuracies obtained from imitation data, instead of treating each task with an infinite accuracy.

TABLE I
COMPARISON OF DIFFERENT PSEUDO INVERSES USED FOR OPERATIONS

$\boldsymbol{J}^{\dagger} = \boldsymbol{J}^T\left(\boldsymbol{J}\boldsymbol{J}^T\right)^{-1}$	**Generalized inverse**
$\boldsymbol{J}^{\dagger} = \boldsymbol{M}^{-1}\boldsymbol{J}^T\left(\boldsymbol{J}\boldsymbol{M}^{-1}\boldsymbol{J}^T\right)^{-1}$	**Weighted generalized inverse**, weighted with the inverse of the mass
$\boldsymbol{J}^{\dagger} = \boldsymbol{\Sigma}_{\ddot{q}}\boldsymbol{J}^T\left(\boldsymbol{\Sigma}_{\ddot{x}} + \boldsymbol{J}\boldsymbol{\Sigma}_{\ddot{q}}\boldsymbol{J}^T\right)^{-1}$	**Bayesian inverse**, weighting and regularization are computed in closed form.

IV. AN OPTIMIZATION POINT OF VIEW

We presented our derivation by prioritizing an operational-space controller and a joint-space controller, however, this was only a special case. Our approach can be generalized to a wider class of problems, where the constraints imposed are linear to the joint acceleration $\ddot{\boldsymbol{q}}$, i.e. can be formulated as

$$\boldsymbol{A}\ddot{\boldsymbol{q}} = \boldsymbol{b}, \tag{12}$$

where the matrix $\boldsymbol{A}$ and vector $\boldsymbol{b}$ possibly depend on the current state of the robot $\boldsymbol{q}$ and $\dot{\boldsymbol{q}}$ at time t. The constraint imposed by the robot's mechanics can be re-formulated in the generalized form of Equation (12), by setting $\boldsymbol{A} = \boldsymbol{J}$ and $\boldsymbol{b} = \ddot{\boldsymbol{x}} - \dot{\boldsymbol{J}}\dot{\boldsymbol{q}}$.

We can now formulate a optimization problem that incorporates a soft version of this constraint while staying close to the prior mean. The covariance matrices serve as L2 norm metric for the objectives, i.e.,

$$\arg\min_{\ddot{q}} J = \arg\max_{\ddot{q}} \; (\boldsymbol{A}\ddot{\boldsymbol{q}} - \boldsymbol{b})^T\boldsymbol{\Sigma}_{\ddot{x}}^{-1}(\boldsymbol{A}\ddot{\boldsymbol{q}} - \boldsymbol{b}) + (\ddot{\boldsymbol{q}} - \boldsymbol{\mu}_{\ddot{q}})^T\boldsymbol{\Sigma}_{\ddot{q}}^{-1}(\ddot{\boldsymbol{q}} - \boldsymbol{\mu}_{\ddot{q}})^T. \tag{13}$$

This formulation resembles the optimization framework presented in [4] with the difference that $\boldsymbol{A}\ddot{\boldsymbol{q}} - \boldsymbol{b}$ is imposed as soft-constraint and not as hard constraint. If we let $\boldsymbol{\Sigma}_{\ddot{x}}$ go to zero, we obtain a hard constraint and all the control laws in [4] can be recovered. However, the pseudo-inverse is lacking a proper regularization which leads to instabilities in singularities. Furthermore, the optimization view does not provide a direct way to update the joint covariance if several tasks need to be prioritized. In contrast, the joint covariance $\boldsymbol{\Sigma}_{\ddot{q}}$ is updated in the Bayesian approach. It specifies the direction in joint space that violate all conditioned task space controllers as little as possible.

A. *Comparison to Strict Prioritization Approaches.*

Our control law can also be formulated for torques $\boldsymbol{u}$ instead of desired accelerations $\ddot{\boldsymbol{q}}$. These derivations are given in the appendix. We observe that the mean $\boldsymbol{\mu}_{\boldsymbol{u}}$ of the controls, given in Equation (14), has a similar structure as well-known operational-space control laws [4], [5], [6], [7], [8], [9], [10], [11], [12]. It consists of a model-based component to compensate for the dynamics of the system, the desired acceleration in the operational-space —which, for example, can be the output of a feedback controller— and a projection component $\left(\boldsymbol{I} - \boldsymbol{J}^{\dagger}\boldsymbol{J}\right)$.

The difference to the aforementioned approaches lays in the computation of the generalized inverse matrix of the Jacobian $\boldsymbol{J}^{\dagger}$. By applying a Bayesian approach, we obtain a generalized inverse matrix of the Jacobian which is both regularized and weighted, while strict prioritization methods use an un-regularized inverse.

The aforementioned approaches can be derived by assuming that the operational-space variance $\boldsymbol{\Sigma}_{\ddot{\boldsymbol{x}}}$ is zero, i.e. $\boldsymbol{\Sigma}_{\ddot{\boldsymbol{x}}} = \lim_{\alpha\to 0} \alpha\boldsymbol{I}$ and, therefore, degrade our approach to a deterministic case. If the operational-space variance is zero, the matrix $\boldsymbol{J}\boldsymbol{J}^{\dagger} = \boldsymbol{I}$ of the projection is a null-space projection, i.e. the lower priority tasks will not interfere with the higher priority tasks. Therefore, decreasing the variance of the operational-space controller $\boldsymbol{\Sigma}_{\ddot{\boldsymbol{x}}}$ can be interpreted as "hardening" the prioritization of the two controllers.

A consequence of not regularizing the generalized inverse is the numerical instability of the inversion at singular kinematic configurations. Some approaches [13], [14] suggest to add a small regularization of the form $\lambda\boldsymbol{I}$ to reduce the numerical instabilities. Performing such a regularization has the physical interpretation of adding a diagonal variance on accuracy of the high priority task. The projection $\left(\boldsymbol{I} - \boldsymbol{J}^{\dagger}\boldsymbol{J}\right)$ will in this case not to be a null-space projection. However, to our knowledge, neither the motivation or the physical interpretation of this regularization has been previously discussed.

By additionally setting the joint-space covariance to $\boldsymbol{\Sigma}_{\ddot{\boldsymbol{q}}} = \boldsymbol{I}$, the pseudo inverse is un-regularized and unweighted and we obtain controls laws as in [4], [5], [6], [7], [8], [9], [10], [12]. Setting the joint-space covariance to $\boldsymbol{\Sigma}_{\ddot{\boldsymbol{q}}} = \boldsymbol{M}^{-1}$, we obtain controllers based on the Gauss principle of least constraint, and consistent to d'Alambert's principle of virtual work [11], [4]. The different approaches for computing the generalized inverse are shown in Table I.

V. Experimental Evaluation

We evaluate our approach on redundant simulated and physical robots performing tasks learned by imitation. As opposed to optimization approaches, our approach does not use a cost function, but learns the desired trajectory distribution from demonstrations. First, we demonstrate that our approach can be used for adapting known tasks, while the reproduction stays in the vicinity of the demonstrations. Second, we show that additional controllers can be smoothly integrated in our framework. Third, we build a library of tasks and show how we can use our approach to learn a combination of tasks with considerably improved data efficiency. We conclude the section by presenting our results on the humanoid platform "iCub" on initiating contacts and while reaching an object.

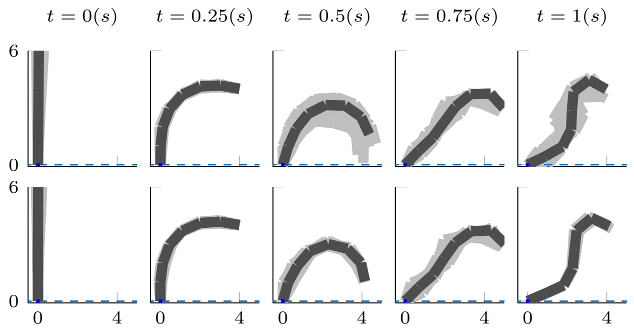

Fig. 2. A visualization of the 7-link planar robot trajectory for different time-steps. The dark configuration denotes the mean configuration. At every evaluation in time, we plot ten samples from the distribution to illustrate the variability of the movement. In the first row, we present the reproduction of the movement after training our approach. In the second row, we present the reproduction of the movement after conditioning at $t = 0.5(s)$ and $t = 1(s)$. We observe that the variance of the task-space movement reduces at the via-points.

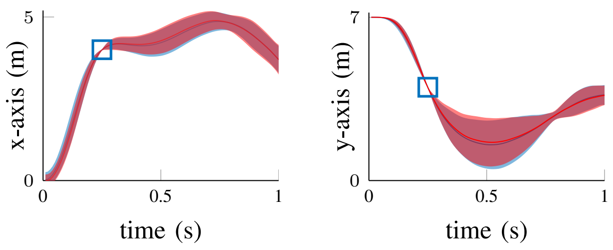

Fig. 3. We present the trajectory distribution of the end-effectors of the 7-link planar robot. The demonstrated trajectory distribution is shown in blue (blue line for the mean and shaded area for two times the standard deviation). The reproduced trajectory distribution that is obtained from our approach is shown in red. The reproduction distribution follows accurately the demonstrated one. The blue boxes illustrate a via-point (low variance of the movement at this time step) that was present during the demonstrations.

A. *Data-Driven Task-Space Adaptation*

In this experiment, we used a planar robot with seven Degrees of Freedom (DoF). We used optimal control to provide demonstrations to our approach. The demonstrations were provided in joint-space. We directly used the joint-space demonstrations for training a ProMP to be used as the lowest priority task. Additionally, we used the task-space trajectories to learn a task-space ProMP. The movement at different time steps is visualized in Figure 2. The demonstrations have different variability at different time-steps throughout the movement. Time step $t = 0.25s$ is a via-point, i.e. has very low variability, in both task-space dimensions. The demonstrated trajectory distribution in task-space is shown in Figure 3(blue), with the trajectory distribution obtained after reproduction(red). The reproduction distribution matches accurately the demonstrations and passes through the via-points. Additionally, we show that our approach can adapt a learned task. The adaptation is performed by using the "conditioning" operation of ProMPs on the task-space primitive. The prior ProMP is not changed by conditioning.

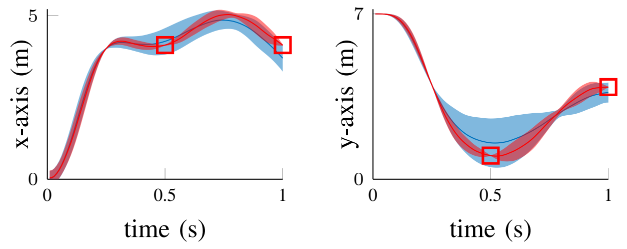

Fig. 4. The trajectory distribution of the end-effectors of the 7-link planar robot after conditioning. In blue, we present the trajectory distribution of the demonstrations. In red, the reproduction after conditioning only the task-space ProMP. The red boxes denote the additional via-points that were not present during the demonstrations. The reproduction can match both, the via-points of the demonstrations and the additional via-points, while it maintains the general shape of the movement. Our approach performs conditioning in task space while it stays close to the demonstrated data in joint space.

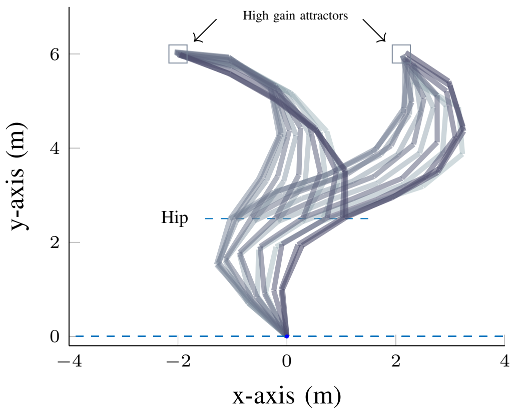

Fig. 5. The planar robot performing a bi-manually reaching task while moving its "hip". The robot accurately stays at the desired targets with its end-effectors during the movement. Additionally, the end of the "hip" link tracks a trajectory with a constant height.

The adaptation does not require to run an inverse kinematics algorithm to find the respective joint configuration, but can be performed directly on the primitive and with a specified accuracy. We present our results in Figure 4, where we added two via-points to the movement. The reproduction can accurately pass through both via-points while it maintains the shape of the movement learned from the demonstrations.

B. Incorporation of External Control Laws

Furthermore, we present our results for a more complex planar robot with two end-effectors. The robot has three links for the torso and five additional links to represent arms. Each link is one meter long. The robot learned a movement where the "hip" moves in a constant height of $2.5m$. We show that expert-knowledge can be incorporated in our approach. The expert designed two feedback controllers with high gains and small variance $\mathbf{\Sigma}_{\boldsymbol{u}} = 10^3$ that attract the end-effectors at $\{2, 6\}(m)$ and $\{-2, 6\}(m)$, for the right and left end-effector respectively. The resulting movement is shown in Figure 5. The robot can perform all of the three tasks; it reproduces accurately the hip movement staying at the desired height and places its end-effectors at the desired locations set by the expert.

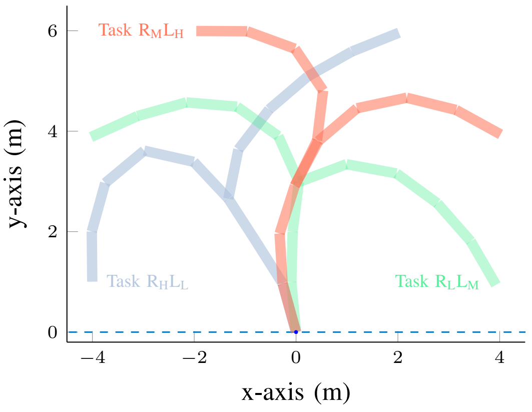

Fig. 6. A visualization of the two end-effector robot we used in our experiments. We present the final configuration, $t = t_{\text{end}}$ of the robot in task space for three different tasks, out of nine tasks we used in the experiment. Each color represents a different task combination. Our approach can learn the task of each end-effector, $\{R_*, L_*\}$, independently. The task of each end-effector, i.e., the reaching of a low point, a mid point, and a high point, is denoted by the L, M, H subscripts.

C. Combining Tasks of Different End-Effectors

In this evaluation we demonstrate the advantages of our approach a combination of tasks for different end-effectors. We use the planar robot with two end-effectors and thirteen DoF. First, we generated demonstrations where each end-effector has the task to reach one out of three end-points at $t_{\text{end}} = 1$. The end-point can either be "low", set at $\{4, 1\}$ for the right end-effector or at $\{-4, 1\}$ for the left, or "mid" at $\{\pm 4, 4\}$, or "high" at $\{\pm 2, 6\}$. The combination of all three tasks of the two end-effectors yields nine different task combinations. For each combination, we generate a set of noisy demonstration. We denote each task by $\{R_i, L_j\}$, where $\{R, L\}$ denotes the end-effector and $i, j \in \{L, M, H\}$ denotes the "low", "mid", or "high" end-point. An illustration of the configuration of the robot at these points is shown in Figure 6. As a baseline, we train nine individual primitives, one for each combination of tasks. However, our approach can use all available demonstrations per task of one end-effector, e.g. $\{L_M, R_*\}$, as it can learn the end-effector tasks independently resulting in a training set per task with three times the number of demonstrations as can be used for the baseline approach. Therefore, our approach considerably outperforms the baseline as the distributions can be estimated with higher accuracy. In Figure 7, we evaluate the average performance of both approaches which was specified as the negative square deviation from the true desired task-space position at the end of the movement. Our approach shows a superior accuracy due to the more efficient data usage. The trajectory distribution for both end-effectors is shown in Figure 8. In this Figure, we show that, using prioritization, we can also reproduce a task combination that has not been demonstrated to the robot.

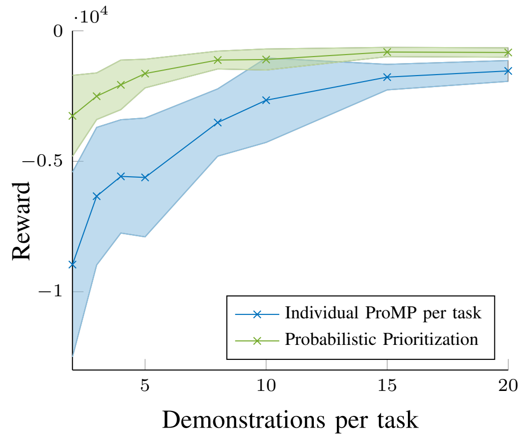

Fig. 7. Comparison between the Bayesian prioritization approach and learning each task independently which is used as a baseline. We vary the number of demonstrations used per task. Using prioritization, we can learn the tasks for each end-effector independently and therefore, can use more training data for the single tasks. For the baseline, we can only learn each combination of the end-effector tasks individually. The plot shows the average negative square deviation from the true desired end-effector position. Using prioritized primitives considerably improves the accuracy of learning due to the more efficient data usage.

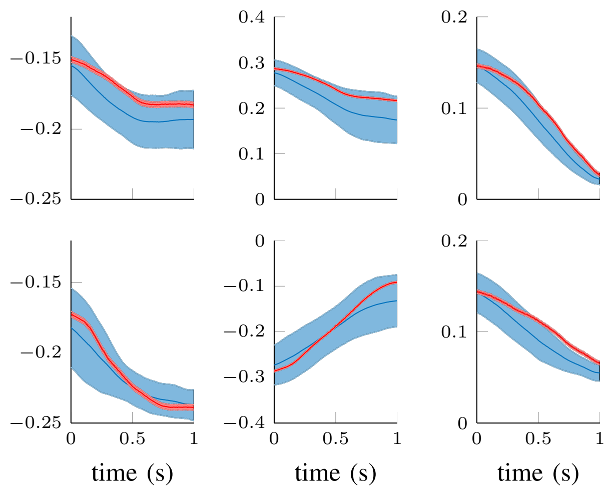

Fig. 9. The trajectory distribution of left (top) and right (bottom) of the iCub robot in Cartesian space, $\{x, y, z\}(m)$ shown in first, second, and third column respectively. We learned prior distribution of is shown in blue. During reproduction, we reached for a "blue—cake" combination (red). The variance of the reproduction distribution is due to the system noise, errors in the dynamics model, and friction.

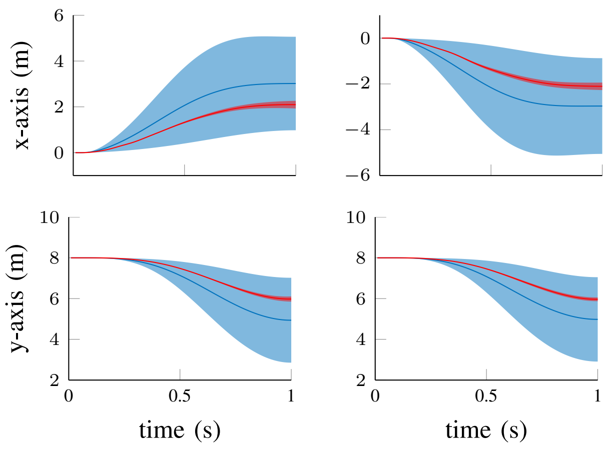

Fig. 8. The trajectory distribution of the end-effectors of the two end-effector robot. The first column presents the left end-effector and the second column of the right end-effector distributions. In blue, we show the prior distribution projected in Cartesian space after training with two task-combinations, $\{R_H, L_M\}$ and $\{R_M, L_H\}$. Our approach utilizes all available demonstrations. In red, we present the reproduction of of the $\{R_H, L_H\}$, a task combination that was not contained in the demonstrations, using our prioritization scheme.

D. *Initiating Contacts during Reaching*

In the final evaluation, we performed an experiment using the humanoid robot iCub to reach objects while improving its stability by partially supporting its weight on a table. The iCub was not mount at a pole, but was rather standing for the duration of our experiments Reaching objects that require the robot to bend the torso can move the center of gravity of the robot out of the support polygon defined by the feet, and, as a result, the robot will loose its balance. The task of the robot is to perform a reaching movement while it initiates a contact to stabilize the robot. The robot reaches for three different objects, as shown in Figure 1, with its right arm. Concurrently, with the left arm, it initiates a contact with the table that increases the stability of the robot. The location of the contact varies over three positions. We provided ten demonstrations reaching for different object locations and initiating different contacts with the forearm of the robot. The robot was capable of reproducing the movements using the prioritized movement primitives, as show in Figure 9. Additionally, the robot could perform unseen combinations of tasks and support locations.

VI. Conclusion

In this paper, we presented a novel approach for movement prioritization based on the combination of Bayesian task prioritization and the Probabilistic Movement Primitives. While prioritization is a well established concept in control, it has not been explored in the context of learning movement representations. We brought attention to the Bayesian task prioritization framework that allows for a principled treatment of the task priorities and avoids numerical instabilities. We combined it with the Probabilistic Movement primitives to enable learning the priorities from demonstrations.

In this paper, we have shown that combining prioritization with learning approaches yields in powerful representation that can be used to solve a combination of tasks with different end-effectors. Our approach is data-driven, i.e., it can solely be trained form demonstrations and minimizes expert knowledge. Especially, it avoids the problem of specifying a cost function for the task in hand, which is still an open problem. We demonstrated that our approach can be used to adapt task-space movements without solving an inverse kinematics problem and, importantly, staying close to the demonstrated data.

A key contribution of our approach is the ability to combine tasks of different end-effectors in a principle and data-efficient way. Our approach can generalize to task combinations that were not present in the demonstrations and requires significantly less training data to achieve the same level of performance.

In future work, we will expand the evaluations of our approach on more complex real-word scenarios. We consider multiple task execution with physical robot interaction under the present of contacts as interesting research direction.

Appendix
Including the Dynamics of the System

The stochastic controller on the joint acceleration given in Equation (7) can be used to control a physical system, i.e. by torque control, using the rigid-body dynamics model [27],

$$\boldsymbol{u} = \boldsymbol{M}(\boldsymbol{q})\ddot{\boldsymbol{q}} + \boldsymbol{C}(\boldsymbol{q}, \dot{\boldsymbol{q}}) + \boldsymbol{G}(\boldsymbol{q}),$$

where $\boldsymbol{M}(\boldsymbol{q})$ denotes the inertia matrix, $\boldsymbol{C}(\boldsymbol{q}, \dot{\boldsymbol{q}})$ denotes Coriolis and centripetal forces, and $\boldsymbol{G}(\boldsymbol{q})$ forces due to gravity. Using the rigid-body dynamics model, we reformulate our controller to operate in the joint torque space, i.e.

$$p_{1|2}(\boldsymbol{u}) = \mathcal{N}\left(\boldsymbol{u}|\boldsymbol{\mu}'_{\boldsymbol{u}}, \boldsymbol{\Sigma}_{\boldsymbol{u}}\right).$$

The mean $\boldsymbol{\mu}_{\boldsymbol{u}}$ of this controller is given by

$$\begin{aligned}\boldsymbol{\mu}'_{\boldsymbol{u}} =& \boldsymbol{M}\left(\boldsymbol{J}^{\dagger}\left(\boldsymbol{\mu}_{\ddot{\boldsymbol{x}}} - \dot{\boldsymbol{J}}\dot{\boldsymbol{q}}\right) + \left(\boldsymbol{I} - \boldsymbol{J}^{\dagger}\boldsymbol{J}\right)\boldsymbol{\mu}_{\ddot{\boldsymbol{q}}}\right) + \boldsymbol{C} + \boldsymbol{G}\\ =& \boldsymbol{M}\boldsymbol{J}^{\dagger}\left(\boldsymbol{\mu}_{\ddot{\boldsymbol{x}}} - \dot{\boldsymbol{J}}\dot{\boldsymbol{q}}\right)\\ &+ \boldsymbol{M}\left(\boldsymbol{I} - \boldsymbol{J}^{\dagger}\boldsymbol{J}\right)\left(\boldsymbol{M}^{-1}\left(\boldsymbol{\mu}_{\boldsymbol{u}} - \boldsymbol{C} - \boldsymbol{G}\right)\right) + \boldsymbol{C} + \boldsymbol{G},\end{aligned}$$

where we used $\boldsymbol{\mu}_{\ddot{\boldsymbol{q}}} = \boldsymbol{M}^{-1}(\boldsymbol{\mu}_{\boldsymbol{u}} - \boldsymbol{C} - \boldsymbol{G})$.

Furthermore, a decoupling of the kinematics and the dynamics can be obtained by setting $\hat{\boldsymbol{\mu}}_{\boldsymbol{u}} = \boldsymbol{\mu}_{\boldsymbol{u}} + \boldsymbol{C} + \boldsymbol{G}$ and using it in place of $\boldsymbol{\mu}_{\boldsymbol{u}}$. In this case, the mean becomes

$$\begin{aligned}\boldsymbol{\mu}'_{\boldsymbol{u}} =& \boldsymbol{M}\boldsymbol{J}^{\dagger}\left(\ddot{\boldsymbol{x}} - \dot{\boldsymbol{J}}\dot{\boldsymbol{q}}\right)\\ &+ \boldsymbol{M}\left(\boldsymbol{I} - \boldsymbol{J}^{\dagger}\boldsymbol{J}\right)\left(\boldsymbol{M}^{-1}\boldsymbol{\mu}_{\boldsymbol{u}}\right) + \boldsymbol{C} + \boldsymbol{G} \quad (14)\end{aligned}$$

which results in the resolved-acceleration controller [28], [29].

References

[1] M. Toussaint and C. Goerick, "A bayesian view on motor control and planning," in *From Motor Learning to Interaction Learning in Robots*, 2010.

[2] A. Paraschos, C. Daniel, J. Peters, and G. Neumann, "Probabilistic movement primitives," in *Advances in Neural Information Processing Systems (NIPS)*, 2013.

[3] A. Paraschos, G. Neumann, and J. Peters, "A probabilistic approach to robot trajectory generation," in *"Proceedings of the International Conference on Humanoid Robots (Humanoids)*, 2013.

[4] J. Peters, M. Mistry, F. Udwadia, J. Nakanishi, and S. Schaal, "A unifying framework for robot control with redundant DOFs," *Autonomous Robots*, 2007.

[5] O. Khatib, "A unified approach for motion and force control of robot manipulators: The operational space formulation," *Journal of Robotics and Automation*, 1987.

[6] O. Khatib, L. Sentis, J. Park, and J. Warren, "Whole-body dynamic behavior and control of human-like robots," *International Journal of Humanoid Robotics*, 2004.

[7] Y. Nakamura, H. Hanafusa, and T. Yoshikawa, "Task-Priority based redundancy control of robot manipulators," *International Journal of Robotics Research (IJRR)*, 1987.

[8] L. Sentis and O. Khatib, "Synthesis of Whole-Body behaviors through hierarchical control of behavioral primitives," *International Journal of Humanoid Robotics*, 2005.

[9] ——, "A whole-body control framework for humanoids operating in human environments," in *International Conference on Robotics and Automation (ICRA)*, 2006.

[10] J. Park, W.-K. Chung, and Y. Youm, "Characterization of instability of dynamic control for kinematically redundant manipulators," in *International Conference on Robotics and Automation (ICRA)*, 2002.

[11] H. Bruyninckx and O. Khatib, "Gauss' principle and the dynamics of redundant and constrained manipulators," in *International Conference on Robotics and Automation (ICRA)*, 2000.

[12] J. Luh, M. Walker, and R. Paul, "Resolved-acceleration control of mechanical manipulators," *Transactions on Automatic Control*, 1980.

[13] P. Baerlocher and R. Boulic, "Task-priority formulations for the kinematic control of highly redundant articulated structures," in *International Conference on Intelligent Robots and Systems (IROS)*, 1998.

[14] ——, "An inverse kinematics architecture enforcing an arbitrary number of strict priority levels," *The Visual Computer*, 2004.

[15] J. Salini, V. Padois, and P. Bidaud, "Synthesis of complex humanoid whole-body behavior: a focus on sequencing and tasks transitions," in *International Conference on Robotics and Automation (ICRA)*, 2011.

[16] J. Salini, S. Barthélemy, P. Bidaud, and V. Padois, "Whole-Body motion synthesis with LQP-Based controller – application to icub," in *Modeling, Simulation and Optimization of Bipedal Walking*, 2013.

[17] W. Decre, R. Smits, H. Bruyninckx, and J. D. Schutter, "Extending iTaSC to support inequality constraints and non-instantaneous task specification," in *International Conference on Robotics and Automation (ICRA)*, 2009.

[18] R. Lober, V. Padois, and O. Sigaud, "Multiple task optimization using dynamical movement primitives for whole-body reactive control," in *International Conference on Humanoid Robots (Humanoids)*, 2014.

[19] ——, "Variance modulated task prioritization in Whole-Body control," in *International Conference on Intelligent Robots and Systems (IROS)*, 2015.

[20] V. Modugno, G. Neumann, E. Rueckert, G. Oriolo, J. Peters, and S. Ivaldi, "Learning soft task priorities for control of redundant robots," in *International Conference on Robotics and Automation (ICRA)*, 2016.

[21] A. J. Ijspeert, J. Nakanishi, and S. Schaal, "Learning attractor landscapes for learning motor primitives," in *Advances in Neural Information Processing Systems (NIPS)*, 2003.

[22] S. Calinon, Z. Li, T. Alizadeh, N. G. Tsagarakis, and D. G. Caldwell, "Statistical dynamical systems for skills acquisition in humanoids," in *Humanoid Robots (Humanoids), 2012 12th IEEE-RAS International Conference on*, Nov. 2012.

[23] S. M. Khansari-Zadeh and A. Billard, "Learning stable nonlinear dynamical systems with gaussian mixture models," *Transactions on Robotics*, 2011.

[24] L. Rozo, S. Calinon, D. Caldwell, P. Jiménez, and C. Torras, "Learning collaborative impedance-based robot behaviors," in *AAAI Conference on Artificial Intelligence*, 2013.

[25] M. Ewerton, G. Neumann, R. Lioutikov, H. Ben Amor, J. Peters, and G. Maeda, "Learning multiple collaborative tasks with a mixture of interaction primitives," in *International Conference on Robotics and Automation (ICRA)*.

[26] E. Rueckert, J. Mundo, A. Paraschos, J. Peters, and G. Neumann, "Extracting Low-Dimensional control variables for movement primitives," in *Proceedings of the International Conference on Robotics and Automation (ICRA)*, 2015.

[27] R. Featherstone, *Rigid body dynamics algorithms*. Springer, 2014.

[28] T. Yoshikawa, *Foundations of robotics: analysis and control*. Mit Press, 1990.

[29] P. Hsu, J. Hauser, and S. Sastry, "Dynamic control of redundant manipulators," in *International Conference on Robotics and Automation (ICRA)*, 1988.

Bibliography

[1] R. Lober, V. Padois, and O. Sigaud. Multiple task optimization using dynamical movement primitives for whole-body reactive control. In *Proceedings of the IEEE-RAS International Conference on Humanoid Robots (Humanoids)*. Madrid, Spain, 2014.

[2] R. Lober, V. Padois, and O. Sigaud. Variance modulated task prioritization in whole-body control. In *Proceedings of the IEEE/RSJ International Conference on Intelligent Robots and Systems*, pages 3944–3949, Hamburg, Germany, Sep 2015.

[3] R Lober, V. Padois, and O. Sigaud. Task compatibility optimization. *IEEE Robotics and Automation Letters*, 2017. Submitted.

[4] V. Modugno, G. Neumann, E. Rueckert, G. Oriolo, J. Peters, and S. Ivaldi. Learning soft task priorities for control of redundant robots. In *Proceedings of the International Conference on Robotics and Automation (ICRA)*, 2016.

[5] Valerio Modugno, Ugo Chervet, Giuseppe Oriolo, and Serena Ivaldi. Learning soft task priorities for safe control of humanoid robots with constrained stochastic optimization. In *Humanoid Robots (Humanoids), 2016 IEEE-RAS 16th International Conference on*, pages 101–108. IEEE, 2016.

[6] A. Paraschos, J. Peters, and G. Neumann. Probabilistic prioritization of movement primitives, 2017. under review.